NAVAL POSTGRADUATE SCHOOL

MONTEREY, CALIFORNIA

THESIS

TENSILE AND FATIGUE FAILURE OF GLASS AND CARBON FIBER BUNDLES

by

Lauren N. Kadlec

March 2022

Thesis Advisor:	Young W. Kwon
Second Reader:	Jarema M. Didoszak

THIS PAGE INTENTIONALLY LEFT BLANK

REPORT DOCUMENTATION PAGE			*Form Approved OMB No. 0704-0188*

1. AGENCY USE ONLY *(Leave blank)*	**2. REPORT DATE** March 2022	**3. REPORT TYPE AND DATES COVERED** Master's thesis

4. TITLE AND SUBTITLE TENSILE AND FATIGUE FAILURE OF GLASS AND CARBON FIBER BUNDLES	**5. FUNDING NUMBERS**
6. AUTHOR(S) Lauren N. Kadlec	
7. PERFORMING ORGANIZATION NAME(S) AND ADDRESS(ES) Naval Postgraduate School Monterey, CA 93943-5000	**8. PERFORMING ORGANIZATION REPORT NUMBER**
9. SPONSORING / MONITORING AGENCY NAME(S) AND ADDRESS(ES) N/A	**10. SPONSORING / MONITORING AGENCY REPORT NUMBER**

11. SUPPLEMENTARY NOTES The views expressed in this thesis are those of the author and do not reflect the official policy or position of the Department of Defense or the U.S. Government.

12a. DISTRIBUTION / AVAILABILITY STATEMENT Approved for public release. Distribution is unlimited.	**12b. DISTRIBUTION CODE** A

13. ABSTRACT (maximum 200 words)

The use of composite materials in naval applications has been increasing, primarily due to their high strength-to-weight ratio. However, additional study is needed on the impact of cyclic loading on these materials. The goal of this study was to develop a mathematical model to predict fatigue failure, so as to be able to more accurately determine material lifetime in naval applications. Fiber bundles of either glass or carbon were used in the testing. Tests under tensile loading were conducted in order to estimate the materials' properties and conduct a slack fiber analysis. Cyclic tests were conducted at strain rates varying from 0.03 to 0.07. The lower end of the cyclic tests was 0.1 times the maximum. Additionally, multi-part tests were conducted. This involved conducting a cyclic test for a certain number of cycles followed by a tensile test to failure. These included both strain-based and force-based cyclic tests. The residual material characteristics were then mathematically modeled in order to predict the fatigue model.

14. SUBJECT TERMS composite materials, cyclic loading, tensile loading, fatigue failure, fatigue model	**15. NUMBER OF PAGES** 67
	16. PRICE CODE

17. SECURITY CLASSIFICATION OF REPORT	**18. SECURITY CLASSIFICATION OF THIS PAGE**	**19. SECURITY CLASSIFICATION OF ABSTRACT**	**20. LIMITATION OF ABSTRACT**
Unclassified	Unclassified	Unclassified	UU

NSN 7540-01-280-5500

Standard Form 298 (Rev. 2-89)
Prescribed by ANSI Std. 239-18

THIS PAGE INTENTIONALLY LEFT BLANK

Approved for public release. Distribution is unlimited.

TENSILE AND FATIGUE FAILURE OF GLASS AND CARBON FIBER BUNDLES

Lauren N. Kadlec
Lieutenant Commander, United States Navy
BS, Webb Institute, 2009

Submitted in partial fulfillment of the
requirements for the degree of

MASTER OF SCIENCE IN MECHANICAL ENGINEERING

from the

NAVAL POSTGRADUATE SCHOOL
March 2022

Approved by: Young W. Kwon
Advisor

Jarema M. Didoszak
Second Reader

Garth V. Hobson
Chair, Department of Mechanical and Aerospace Engineering

THIS PAGE INTENTIONALLY LEFT BLANK

ABSTRACT

The use of composite materials in naval applications has been increasing, primarily due to their high strength-to-weight ratio. However, additional study is needed on the impact of cyclic loading on these materials. The goal of this study was to develop a mathematical model to predict fatigue failure, so as to be able to more accurately determine material lifetime in naval applications. Fiber bundles of either glass or carbon were used in the testing. Tests under tensile loading were conducted in order to estimate the materials' properties and conduct a slack fiber analysis. Cyclic tests were conducted at strain rates varying from 0.03 to 0.07. The lower end of the cyclic tests was 0.1 times the maximum. Additionally, multi-part tests were conducted. This involved conducting a cyclic test for a certain number of cycles followed by a tensile test to failure. These included both strain-based and force-based cyclic tests. The residual material characteristics were then mathematically modeled in order to predict the fatigue model.

THIS PAGE INTENTIONALLY LEFT BLANK

TABLE OF CONTENTS

THIS PAGE INTENTIONALLY LEFT BLANK

LIST OF FIGURES

LIST OF TABLES

THIS PAGE INTENTIONALLY LEFT BLANK

LIST OF ACRONYMS AND ABBREVIATIONS

E	young's modulus
EFM	elemental failure method
FAA	Federal Aviation Administration
FEA	finite element analysis
MTS	materials test system
PLA	polylactic acid
RVE	representative volume elements
SEM	scanning electron microscopy

THIS PAGE INTENTIONALLY LEFT BLANK

ACKNOWLEDGMENTS

First and foremost, I would like to thank Professor Young Kwon, my advisor. Dr. Kwon provided invaluable guidance and knowledge throughout the entire research and writing process. Additionally, I would like to thank Professor Oleg Yakimenko for providing MATLAB support for testing analysis, Assistant Professor Jarema Didoszak for his assistance with 3D printing, and Dr. Chanman Park for his machinery expertise and assistance with testing. In closing, I would like to thank my family and friends for their support.

THIS PAGE INTENTIONALLY LEFT BLANK

I. INTRODUCTION

A. COMPOSITE MATERIALS

Composite materials can be defined as "solid materials composed of a binder or matrix that surrounds and holds in place reinforcements" [1]. While binders are predominantly polymer-based, metals and ceramics can also be used. The binder can also be referred to as the matrix or resin. While reinforcements are predominantly fiber, emerging materials for that function include particle fillers and nano fillers. The focus for this study is on fiber reinforcements for use in polymer-based binders. Advantages of composites include a high strength-to-weight ratio, good fatigue resistance, and ease of customization. Disadvantages of composites include higher cost and higher length of time to manufacture [1]. The fibers bear the majority of the load in the composites. Therefore, the bond between the fibers and matrix must be adequate for load transfer from the matrix to the fibers. The primary functions of the matrix are to bind and shield the fibers.

Given that the strength of the composite comes predominantly from the fibers, the manner in which the fibers are arranged can result in directionally specific strength property. For example, if all fibers are laid in one direction, then the composite will be strongest in that direction. Use of a multilayered grid, or laminate, with differing fiber directions would result in more uniform strength properties. Building the components up to this type of laminate is shown in Figure 1. It shows how the fibers and resin are two different components that are combined to create a composite layer. Several composite layers can then be combined, potentially with fibers oriented in different directions, to form a laminate.

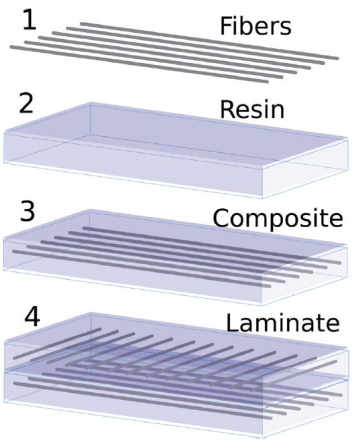

Figure 1. Building Blocks of Composites. Source: [2].

The initial use of composites in military applications occurred in World War II. Composites were used in maritime applications in order to attempt to mitigate corrosion issues seen in metals and wood [3]. Lower weight was an additional benefit of that use. For aircraft, the reason for use at that time was actually due to concerns of lack of metal availability, so exploration into metal alternatives was conducted [1]. Research and continued use in both military and civilian applications following the war led to the reasoning being more for their advantageous properties.

Composites continue to increase in popularity for ships and aircraft, both military and civilian. Currently, composites can be found in military maritime applications such as hulls, propellers, hatches, railings, valves, and domes, and military aircraft applications such as skins, blades, propellers, and fuselages [3, 4]. The Boeing 787 is the first aircraft to use over 50% composites [2]. On the F-35, carbon fiber composites comprise 35% of the total weight, the majority of which is the skin [5]. The reason for the lack of use in more structural application is the increased cost for composites used in load bearing applications. For such applications the weight savings does not necessarily outweigh the additional cost impact, unlike for the aircraft skin. Additionally, the safety for use in aircraft must also be examined. The Federal Aviation Administration (FAA) has set criteria for evaluation of fatigue and damage tolerance [6]. Fatigue failure is where a crack occurs due to fatigue loading, which then propagates under continued loading, resulting in eventual failure once

a critical crack size is reached. Evaluation of fatigue failure is especially critical, as this is the most common cause of failure of composites [7].

B. FATIGUE

Fatigue occurs when an item is subjected to repeated or fluctuating stresses. This is common in applications such as bridges, aircraft, and machine components [8]. The latter two are the military applications in which fatigue is frequently seen. Fatigue failure can occur at a stress much lower than the yield strength for a material. The failure method in fatigue failure is usually initiation of cracks followed by their propagation until material failure. Due to this, it is important to be able to predict the conditions under which the failure will occur. Laboratory testing can be used to create a plot of stress amplitude versus number of cycles to failure for cyclic loading. This plot is known as an S-N curve, and can be a useful tool for predicting the lifetime of a material under cyclic loading. Materials can also be broken down into two groups by whether or not they have a fatigue limit. A material with a fatigue limit will have a limiting stress amplitude below which no fatigue failure will occur, regardless of the number of cycles, as shown in Figure 2. For a material without a fatigue limit, the stress amplitude continues to decrease as the number of cycles increases, as shown in Figure 3. Ferrous metals, such as steel, typically have a fatigue limit, making their failure criteria easier to predict. However, nonferrous metals and composites typically do not have a fatigue limit. Therefore, examining fatigue failure models is key for such materials.

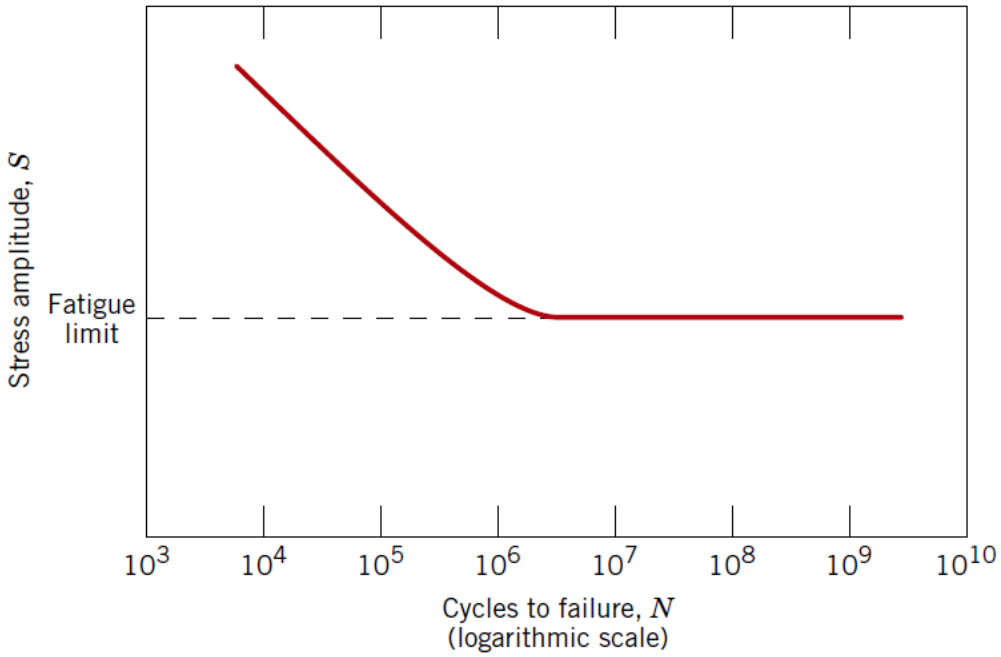

Figure 2. S-N Curve with a Fatigue Limit. Source: [8].

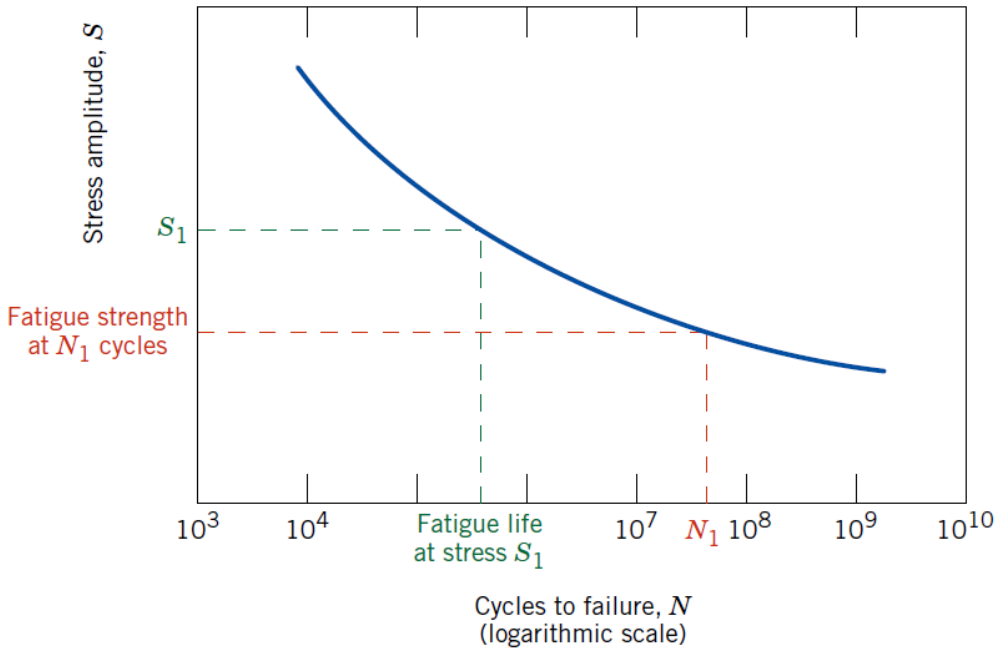

Figure 3. S-N Curve without a Fatigue Limit. Source: [8].

C. PRE-EXISTING FATIGUE FAILURE MODELS

During cyclic testing of any material, micro-cracks can initiate during the initial loading. In an isotropic material such as metal, those micro-cracks would propagate into dominant cracks, resulting in failure. Therefore, for isotropic materials dominant cracking is the predominant cause of failure and therefore controls strength. However, in most composites, even with the micro-cracks, the composite can still sustain the load until final failure [9, 10]. Therefore, fiber failure is likely to be the most common failure mode for these materials. In addition to fiber failure, other possible failure modes are matrix cracking, delamination, and fiber/matrix interface debonding or fiber pullout [11, 12, 13].

Additionally, the orientation of the fibers relative to the material loading can impact the fatigue strength. For example, for a composite loaded at a ±45° in relation to the fibers versus one loaded in line with the fibers, the latter will have a higher fatigue strength. Therefore, a transverse tensile load on a composite object can result in failure at a lower than expected strength [14].

Modeling of fatigue failure in composites is more complicated than in metals, as composite failure can involve more than one mode of failure simultaneously. Most existing models use either a micromechanics scale or a macromechanics scale. A micromechanics scale can also be referred to as using an elemental failure method (EFM) [11]. In this case, fibers within the composite are modelled individually. However, factors such as local fiber concentration and variations in crack size can render this methodology less effective. A machromechanics method uses representative volume elements (RVE), which means looking at a volume of the composite across a multitude of fibers [11]. This helps to account for variations in both the fibers themselves and in the flaws/cracks. However, this methodology still needs to be explored further for better understanding, as it relies predominantly on fiber failure being the primary failure mode.

Existing testing has also shown that there is a potential relationship between static strength and fatigue life for a composite loaded in line with the fiber orientation [9, 15]. Based on this, degradation of a fiber sample should be directly determinable from test data. However, this would also rely on fiber failure being the primary failure mode and not

account for the potential of premature failure due to fiber pullout [9]. Additional models attempt to use a statistical approach to determine strength versus fatigue life. A sudden death approach assumes that the strength remains constant under cyclic loading, until a drastic degradation in the final few cycles before failure. Under an assumption of residual strength, residual strength is a monotonically decreasing function over fatigue life [10, 16]. Many current models assume that the rate of change is a "power function of the fatigue cycle, n, and proportional to a parameter which is a function of damage" [10]. However, these statistical approaches still do not typically account for the potential of more than one failure mode.

For an example of a composite with behavior that would not be modeled well under the previous examples, short-fiber composites are gaining in popularity. In this form, fiber failure will not necessarily be the failure mode, matrix cracking can also play a major role. Therefore, micro-cracks can directly result in failure in a short fiber composite. Even with this drawback, they are "an attractive candidate for load-bearing structural applications due to the advantages in processability, high-volume production, parts consolidation, lower tooling costs, favorable mechanical properties, and increased flexibility in design" [17]. Additionally, high cyclic stress and low cyclic stress can result in different schemes towards failure. High cyclic stress causes a higher microcrack density with a lower characteristic crack length, whereas low cyclic stress causes the opposite. Therefore, newer type composites such as these also need to be properly accounted for in fatigue failure models.

The most applicable of the statistical models apply the concepts of both critical elements and subcritical elements. The critical element is the primary contributor to failure, such as the fibers if fiber failure is the primary mode of failure. The subcritical elements are those which do not directly contribute to the primary failure mode, but have failure which contributes to a redistribution of local stress. For example, the matrix would be a subcritical element as matrix cracking would cause a redistribution of the local stress on the fibers. While the profile of strength degradation is determined by the critical elements, it must be scaled appropriately to account for the subcritical elements [13]. The local

stresses caused by the subcritical elements still play a key role in the overall performance of the composite [18].

D. CURRENT FATIGUE FAILURE MODELS

More current modeling uses a multiscale approach to predict overall material properties, or macro-scale properties, based on the constituent material properties, or micro-scale properties. The methodology involves conducted testing on the constituents, in this case the fibers and matrix, and then scaling them properly to predict the overall materials properties of the composite. For example, fiber/matrix interface debonding would not be reflected in either of the constituent testing, but would need to be accounted for in the scaling [19]. The scaling approach is referred to as the unit-cell model, as shown in Figure 4. In this approach, the micro-scale properties are upscaled to the macro-scale properties to predict the overall composite properties. The predecessor thesis to this thesis attempted to use testing to "relate the number of cycles until failure to the changing modulus of elasticity of the material" [20]. This included testing on both fibers and whole composites.

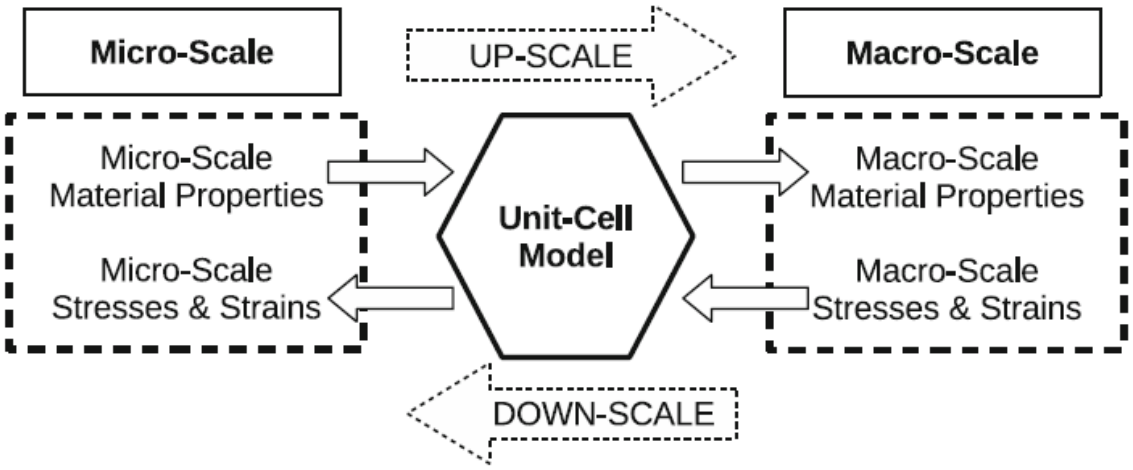

Figure 4. Multiscale Approach Using Unit-Cell Model. Source: [19].

THIS PAGE INTENTIONALLY LEFT BLANK

II. EXPERIMENTAL SETUP

A. TEST MACHINERY

All testing was conducted on the materials test system (MTS), model number 359-LVDT. The test system is supported by an electronic controller and a hydraulic grip system, as shown in Figure 5. The electronic controller and its attached computer allow for setting up and conducting the test, such as type of test (cyclic or tensile) and parameters such as maximum and minimum values for cyclic tests and rate of test for tensile tests. The computer also saves a text file of data for each test, which can then be downloaded for further analysis. The hydraulic grip system controls the setting and releasing of the grip and also the grip strength used.

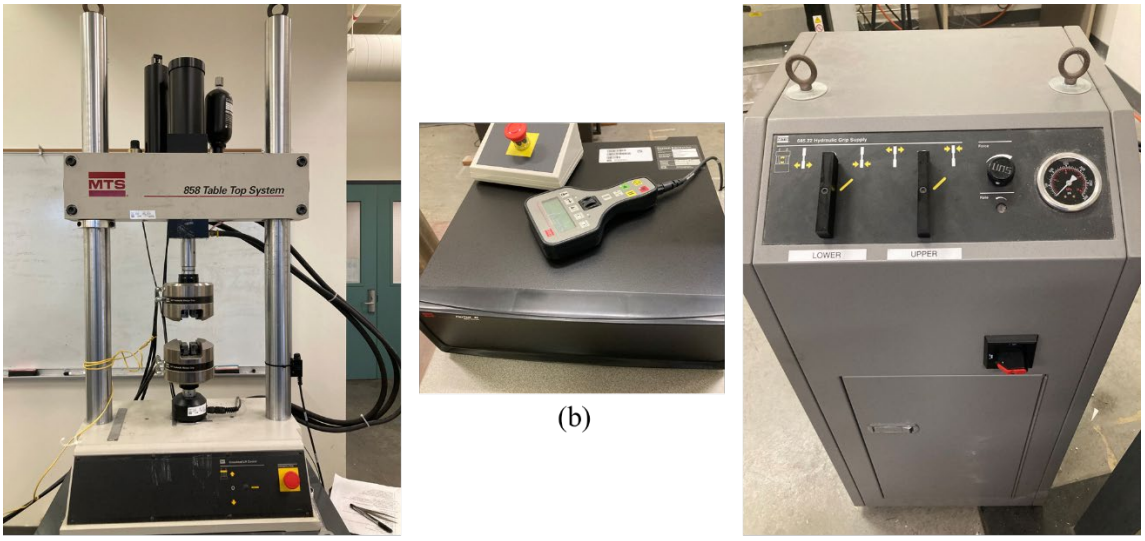

(a) (b) (c)

Figure 5. MTS Test Equipment, (a) MTS Model 359-LVDT, (b) Electronic Controller, (c) Hydraulic Grip System

B. ADAPTERS

1. Geometry Iterations

Given the grip setup of the MTS, it is not feasible to directly mount fiber bundles. Therefore, adapters had to be used in order to conduct testing on the fiber bundles. While all of the cyclic tests were conducted with the adapters mounted horizontally, a few of the tensile tests on the initial adapter types were conducted with the adapters mounted vertically, as per Figure 6. However, all of the tensile tests conducted using the steel adapters were performed in a horizontal mounting. Several iterations were used in order to find a size/material combination that had minimal deflection during testing, as shown in Figure 7. Fiber bundles were mounted by taping the end of the bundle diagonally across the rectangular portion and then wrapping the bundle around the circular portion of the adapter. The diagonal lines on the adapters in Figures 7(c) and (d) are remnants from the fiber bundles mounted to them. With the exception of a few tests, all testing was conducted with two full wraps of fiber bundle around the adapter. The small polylactic acid (PLA) adapters (Figure 7(a)), which were 3D printed with a 20% fill, were leftovers from a previous thesis on fiber testing [20]. This smaller geometry is per Figure 8. However, these adapters were both compressed by the grip strength and had visible deflection during testing. In Figure 7(a), the width of the tab portion is wider than diameter of the bottom circle due to that grip strength compression. The original geometry of these was with the tab width equal to the bottom circle diameter, per Figure 8. The next iteration was the same geometry but using 3D printed polycarbonate, also with a 20% fill (Figure 7(b)). While these did not compress under the grip strength, they still visibly deflected during testing. The third iteration (Figure 7(c)) was to increase the geometry where possible and also fillet edges to try avoid local stress concentrations, as shown in Figure 9. The 60.325 mm (2.375 in) along the base remained unchanged in order to retain the ability to test vertically without having the adapter, other than the circular portion, stick out excessively from the hydraulic grips on the MTS. The width was kept to 25.4 mm (1 in) so that entire rectangular portion would be held inside of the grip in a horizontal mounting. Therefore, to keep the width consistent the diameter of the circular portion for wrapping the fiber bundles was also increased to 25.4 mm (1 in). The rectangular portion could be no taller than the 6.35 mm

(0.25 in), as once the tape to hold the fiber bundles on was added, this was the maximum size that would still fit into the grip. In addition, these larger polycarbonate adapters were printed with 90% fill. While the deflection during testing was lower, it was still visibly noticeable. The final iteration (Figure 7(d)) was to make the larger geometry out of machined steel. There was no noticeable deflection during testing and this adapter type was used for all remaining testing.

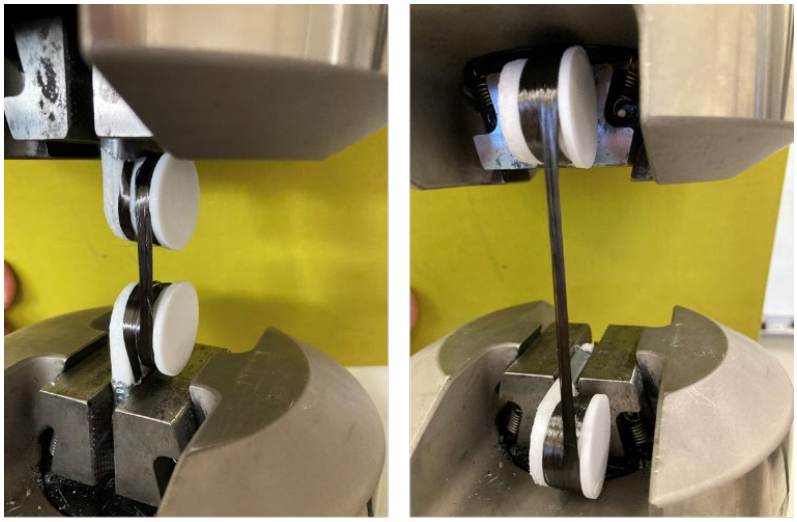

(a) (b)

Figure 6. Mounted Adapters, (a) Vertical Mounting, (b) Horizontal Mounting

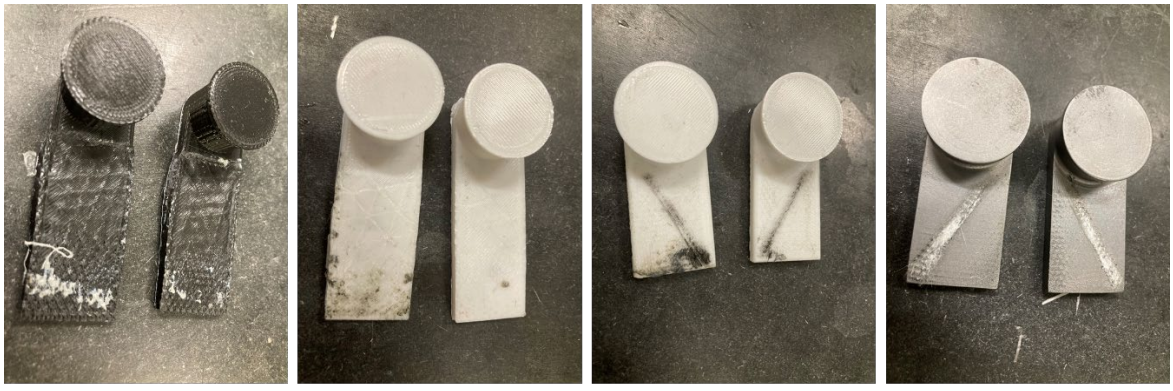

(a) (b) (c) (d)

Figure 7. Testing Adapters, (a) PLA – small, (b) Polycarbonate – small, (c) Polycarbonate – large, (d) Steel – large

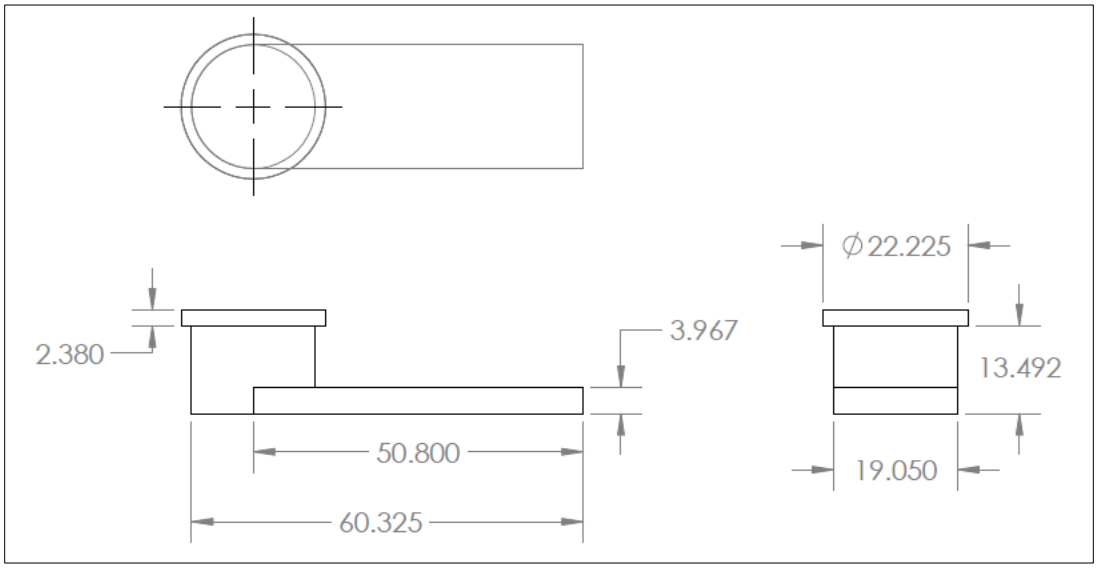

Figure 8. Smaller Adapter Geometry (Units: mm)

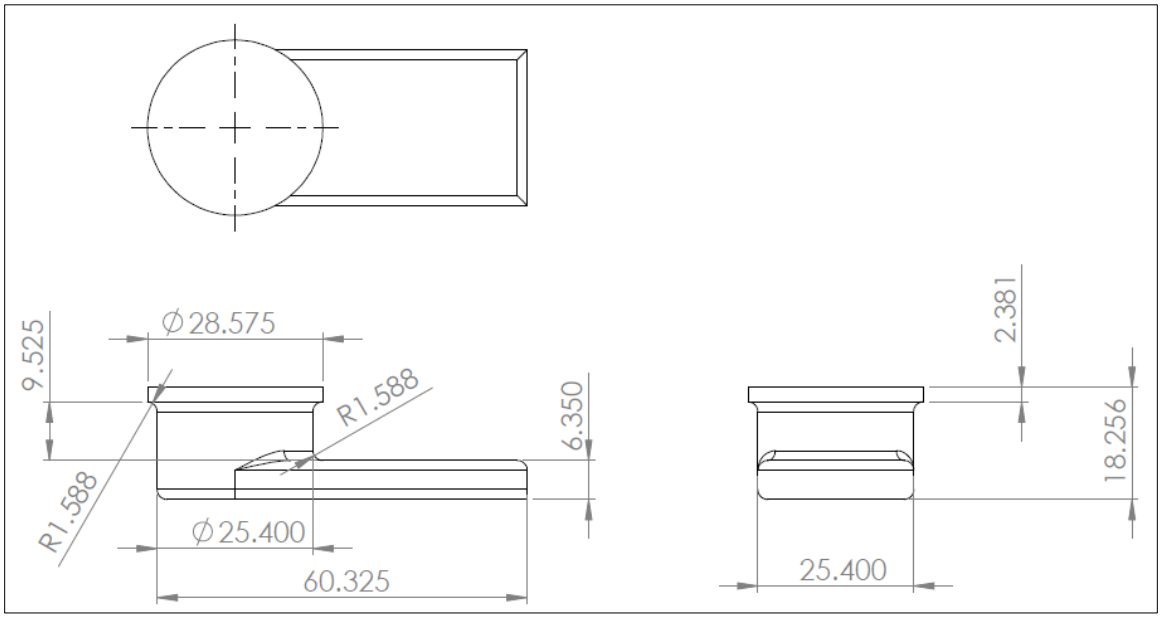

Figure 9. Larger Adapter Geometry (Units: mm)

2. Ansys Analysis

In order to further examine the amount of deflection in the adapters during testing, finite element analysis (FEA) via computer modeling was conducted in Ansys for the two larger geometry adapters in a horizontal mounting. The goal was to see if any adapter type achieved a deflection lower than 0.1 mm (0.00394 in). In order to replicate only the portion that extends outside of the machine grip, the overall length was decreased from 60.325 mm (2.375 in) to 32.544 mm (1 9/32 in), as shown in Figure 10. The rectangular face at which the virtual cut occurred (located in the Y-Z plane per the pictured axis in Figure 10) was treated as a fixed face, as this is where the adapter would be emerging from the machine grip. At the time of this analysis, the maximum force reached during testing was 775 kN. In order to account for any potential changes in test method, a factor of 2 was applied. Therefore, a point load of 1550 kN, located where the fiber bundle would be coming off the adapter, was used for the FEA. For polycarbonate, a rectangular piece of polycarbonate, measuring 101.6 mm (4 in) by 25.4 mm (1 in) by 6.35 mm (0.25 in) was 3D printed in order to conduct a tensile test to find the young's modulus (E) of the material. The 25.4 mm (1 in) by 6.35 mm (0.25 in) cross section was in order to mirror the cross section of the rectangular portion of the larger adapters. The setup of this test is per Figure 11. Considering that the larger polycarbonate adapters were printed at 90% fill, the goal of this test was to see if an experimental young's modulus for 90% fill would yield different results from Ansys's default young's modulus for polycarbonate, which is likely for solid polycarbonate. Three FEA runs were therefore conducted: polycarbonate with the Ansys default young's modulus of 2.38e9 Pa, polycarbonate with the experimental young's modulus of 1e9 Pa, and steel with the Ansys default young's modulus of 2e11 Pa. While they all experienced a similar maximum stresses, the steel adapter was the only adapter that remained below the desired maximum deflection of 0.1 mm, as per Table 1. As expected given the use of the same applied force, the distribution of deformation was comparable between the samples, as per Figures 12 and 13.

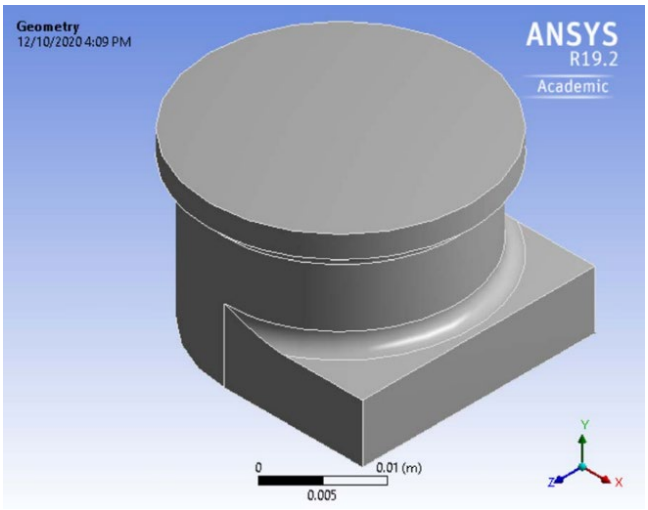

Figure 10. Isometric View of Adapter Portion for Ansys Analysis

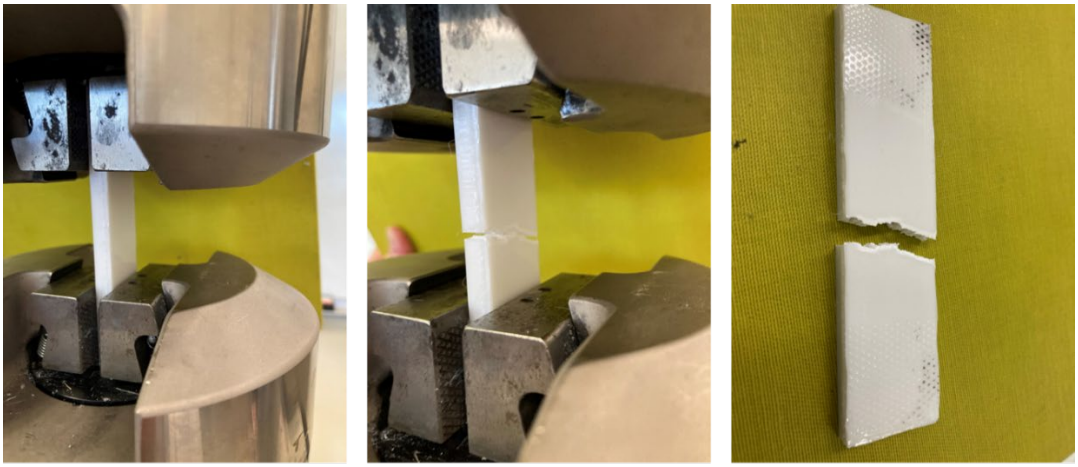

(a) (b) (c)

Figure 11. Polycarbonate Tensile Test, (a) Initial Test Setup, (b) Post-Test, (c) Broken Sample after Removal

Table 1. FEA Results for Polycarbonate and Steel Adapters

Material	E (Pa)	Max Deflection (mm)	Max Stress (Pa)
Polycarbonate	2.38e9	0.670	1.42e8
Polycarbonate	1e9	1.60	1.42e8
Steel	2e11	0.00795	1.46e8

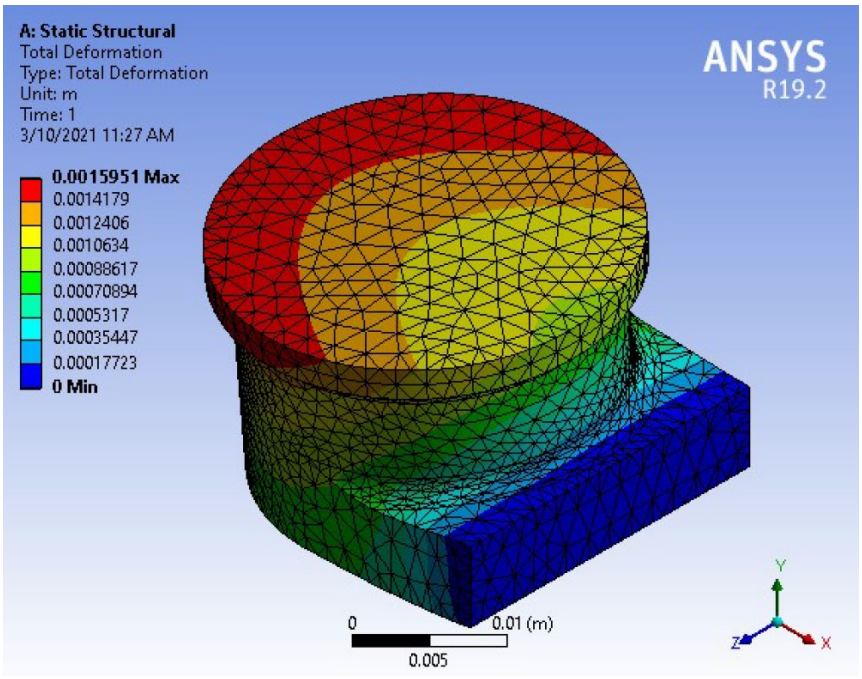

Figure 12. Distribution of Deformation in Polycarbonate Adapter using Experimental Young's Modulus

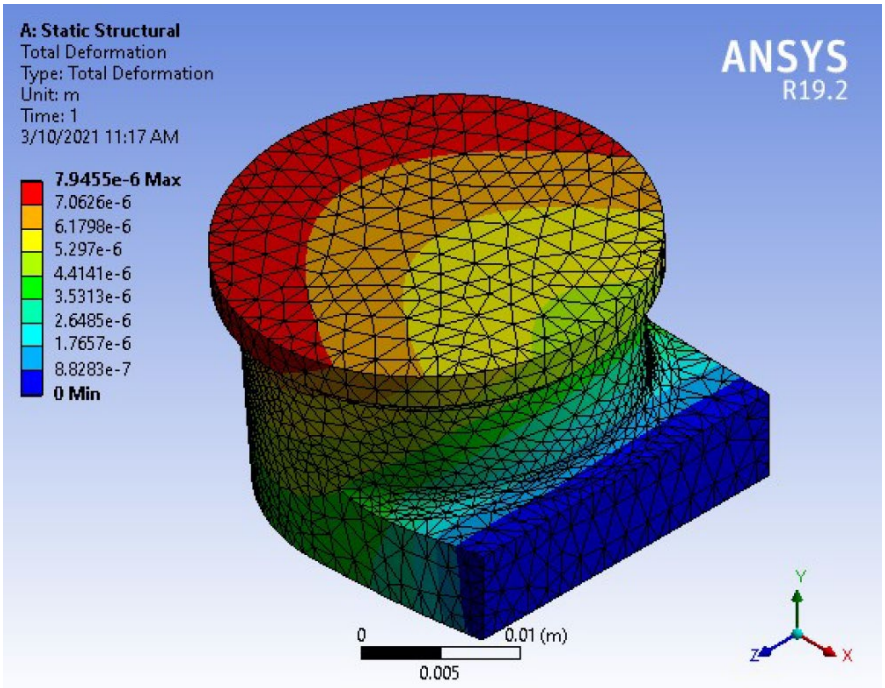

Figure 13. Distribution of Deformation in Steel Adapter

C. TESTING SETUP

While there were some differences in setup by type of testing, there were a few parameters that remained the same. While some early testing was conducted with a 5 MPa grip strength, slippage issues occurred using this value. Therefore, the majority of testing used a 10 MPa grip strength. Additionally, all tests were run taking 16 data sampling points per second.

(1) Tensile Testing Setup

Initial tensile testing occurred with the adapters in a vertical orientation, as the initial iterations of the adapters saw too much deflection when used in a horizontal orientation. However, tensile testing in the later iterations of adapters were conducted in the horizontal orientation in order to match the orientation used in the cyclic and multi-part test types. All tensile tests were conducted at a testing rate of 2 mm/min.

(2) Cyclic Testing Setup

The setup for cyclic testing was displacement based to a specific initial strain. The initial strain was set between 0.03 and 0.07. The maximum displacement for the cycle was that to meet the specified initial strain. The minimum displacement was set to 10% of the maximum displacement. This type of cyclic testing was conducted by applying the load at a testing rate of 2 Hz.

(3) Multi-part Testing Setup

Multi-part testing was conducted by running a force-based or a strain-based cyclic test for a specified period of time and then running a tensile test until failure to find the residual strength. The testing parameters for the strain-based cyclic and tensile portions of the testing matched the parameters discussed above for individually conducting a strain-based cyclic test or tensile test. For the force-based cyclic portions, the maximum force used ranged between 0.85kN to 1kN. Minimum force was set to 10% of the maximum force. The previously used testing rate of 2 Hz did not allow for the test to reach its maximum point, so after some experimentation a rate of 0.25 Hz was used.

III. EXPERIMENTAL RESULTS

A. GLASS FIBER TEST RESULTS

1. Tensile Tests Results

One tensile test, using the smaller polycarbonate adapters, was conducted, as shown in Figure 14. The results from this test are further analyzed later while discussing slack fiber behavior.

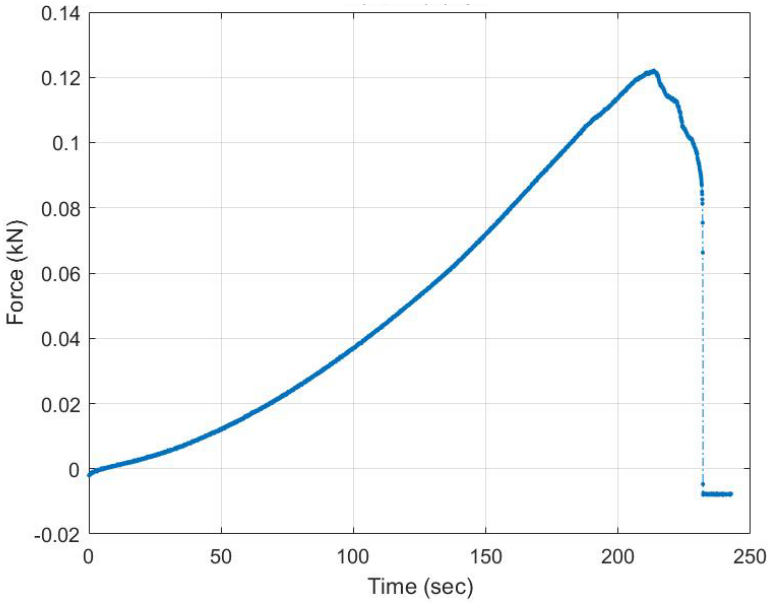

Figure 14. MTS Data for Glass Fiber Tensile Test

2. Cyclic Test Results

Several issues were encountered during glass fiber cyclic testing. For example, with tests run at a low strain rate, failure was not achieved and the bottom of the force curve increased rather than staying at or near zero. The inability to reach failure is likely the result of test methodology. Glass fibers have some elasticity, so with low max displacement corresponding to a low strain rate, the elastic capability of the fibers is never exceeded. This is evident in the graphical output from the MTS, as the minimum force increases and the difference between minimum force and maximum force in a cycle decreases until it

maintains a steady constant value, as in Figure 15. Therefore, the low maximum strain values are insufficient to properly test the glass fibers, as it likely means the testing is occurring at displacements too low for all fibers to become taut and loaded due to the twisting in the fiber bundles. Data was collected at strains from 0.03 to 0.07 in increments of 0.01, as per Table 2. In addition to the data collected from the graphical peak, data was also collected on number of cycles it took to reach 70% of the maximum force and 40% of the maximum force. Of note, all of these tests were conducted with PLA or polycarbonate adapters and 40% of the maximum force was not reached during testing with a maximum strain of 0.03 or 0.04. Additionally, there seemed to be a lack of consistency in the collected data. While all tests reached their peak force in a similar number of cycles, there was a lack of consistency in what that force was and then how many cycles it took to reach both 70% and 40% of that force. An example of the level of error was calculated for a few data points on the tests conducted at a strain of 0.07, as in Table 3. Percent errors were calculated based on the value found in the first test listed. Based on these issues with the prescribed test method, additional testing of glass fibers was not conducted and the focus was placed on carbon fiber testing. However, this portion of testing was still valuable as it assisted with areas such as development of proper adapters and testing methodology.

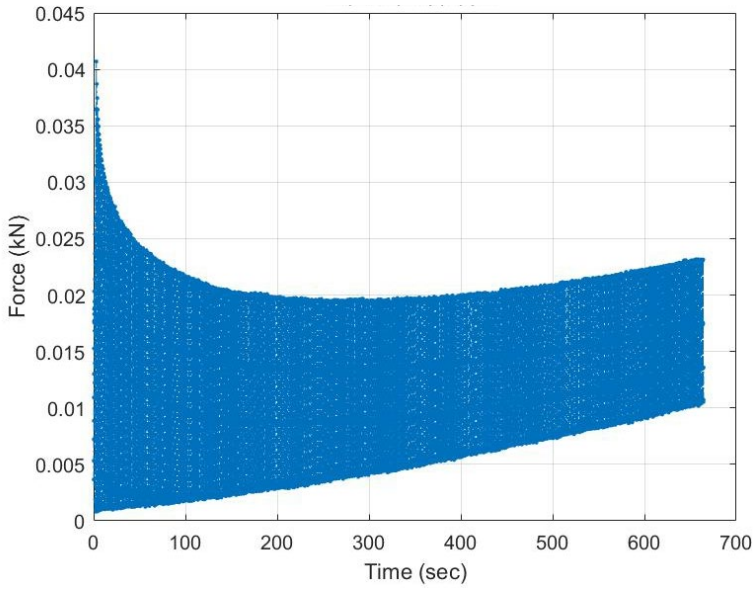

Figure 15. MTS Data for Glass Fiber Cyclic Test with Maximum Strain of 0.03

Table 2. Glass Fiber Test Data from Strain-based Cyclic Tests

Max Strain	Max Force (kN)	No. of Cycles to Peak	70% Force (kN)	No. of Cycles to 70% Force	No. of Cycles from Peak to 70% Force	40% Force (kN)	No. of Cycles to 40% Force	No. of Cycles from Peak to 40% Force
0.03	0.0407	5.89	0.0285	37.90	32.01	0.0163		
	0.0555	5.89	0.0388	123.90	118.01	0.0222		
	0.0465	5.89	0.0325	133.90	128.01	0.0186		
	0.0366	5.89	0.0256	37.88	31.99	0.0146		
	0.0354	5.77	0.0248	35.76	29.99	0.0142		
	0.0310	5.77	0.0217	30.76	24.99	0.0124		
	0.0294	5.77	0.0205	40.76	34.99	0.0117		
	0.0267	5.89	0.0187	44.80	38.91	0.0107		
0.04	0.0541	5.78	0.0379	134.86	129.08	0.0217		
	0.0503	5.89	0.0352	107.88	101.99	0.0201		
	0.0558	5.89	0.0390	103.88	97.99	0.0223		
0.05	0.0787	5.78	0.0551	50.78	45.00	0.0315	47.00	94.00
	0.0657	5.92	0.0460	57.90	51.98	0.0263	75.99	151.98
	0.0603	5.81	0.0422	72.82	67.01	0.0241	92.51	185.03
	0.0673	5.80	0.0471	62.82	57.02	0.0269	115.50	231.00
	0.0644	5.95	0.0451	48.94	42.99	0.0258	103.02	206.05
0.06	0.0890	5.76	0.0623	18.76	13.01	0.0356	38.01	76.02
	0.0647	5.80	0.0453	61.80	56.00	0.0259	88.49	176.98
	0.1078	5.79	0.0755	14.80	9.00	0.0431	12.50	25.01
	0.0995	5.88	0.0697	29.88	24.00	0.0398	38.99	77.98
	0.0689	5.81	0.0482	18.82	13.01	0.0275	68.49	136.99
0.07	0.1080	5.79	0.0756	20.80	15.01	0.0432	12.99	25.99
	0.1349	5.80	0.0944	17.81	12.01	0.0540	16.49	32.98
	0.0694	5.83	0.0485	59.82	53.99	0.0277	98.98	197.97

Table 3. Error Analysis for Cyclic Tests Conducted at a Strain of 0.07

Max Force (kN)	% Error	No. of Cycles to 70% Force	% Error	No. of Cycles to 40% Force	% Error
0.1080		20.80		31.78	
0.1349	24.9%	17.81	-14.4%	38.78	22.0%
0.0694	-35.8%	59.82	187.6%	203.80	541.3%

B. CARBON FIBER TEST RESULTS

All fiber testing was conducted based on the premise of evaluating behavior in the midsection of the fiber, which was done by placing marks on the fiber to indicate the portion being used for evaluation and to be able to record a tested length, as in Figure 16. Fiber failure was not necessarily indicated by complete separation. Complete separation was only seen when failure occurred in the fibers at the adapters, for which tests were discounted as this was not failure in the evaluated section. For failure in the midsection, fibers were pulled/stretched to the point that they could no longer bear a load. This was observable in that the intact fibers had a straight, shiny appearance whereas the pulled fibers had a more thin and tangled appearance. While this was observable via the naked eye, it was viewed via optical microscopy for greater contrast, as in Figure 17. Additionally, effort was made while mounting the samples to align fibers and remove slack as much as possible, but not all slack could be avoided. This is due to the fact that fiber bundles were manufactured with the fibers in a twisted or tangled manner. This was observable via both optical microscopy and scanning electron microscopy (SEM), as in Figure 18. While pre-tensioning for testing was considered, it was decided against as it would then place excessive stress on some fibers prior to the start of a test. A statistical model for slack fiber behavior is discussed later.

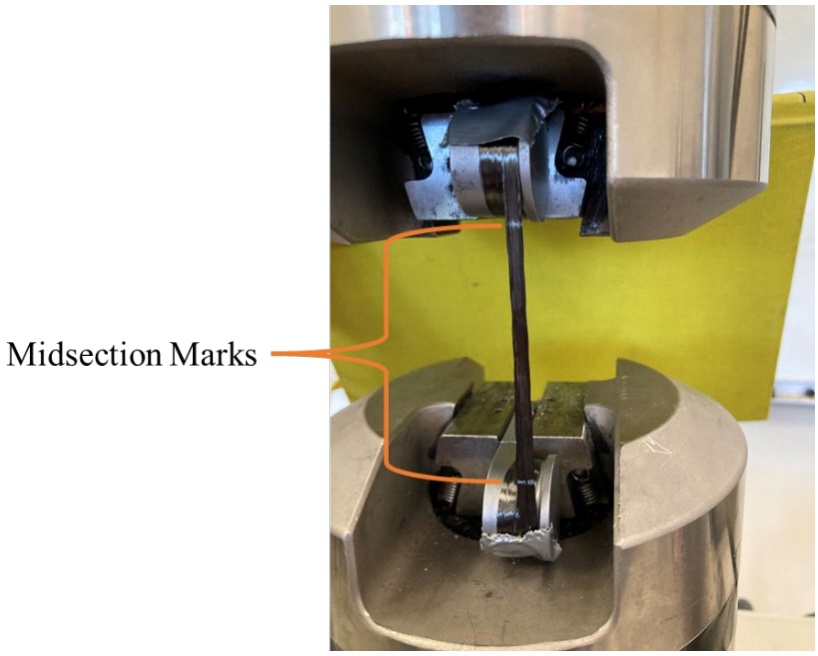

Figure 16. Testing Length Marks on Midsection of Fiber Bundle

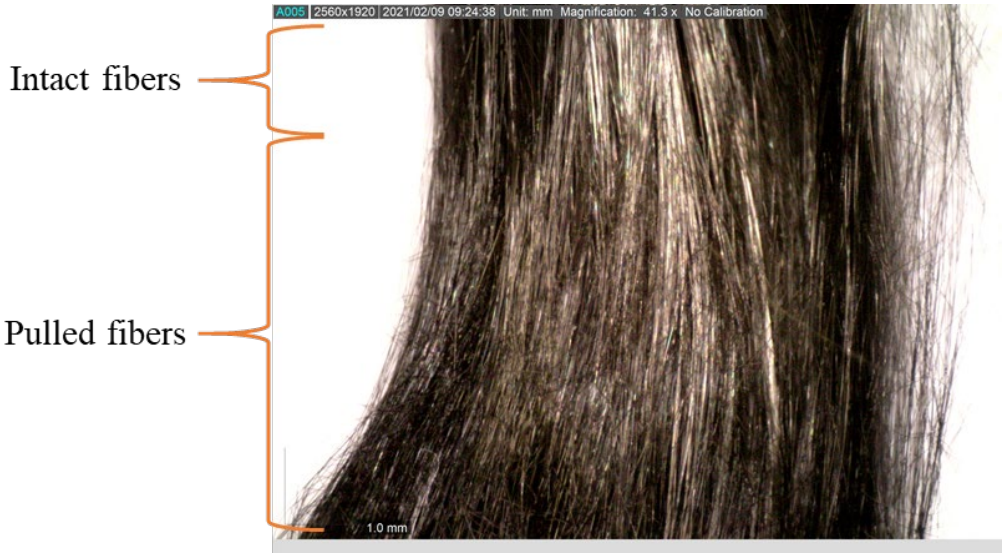

Figure 17. Failure Mode of Pulled Fibers via Optical Microscopy

(a) (b)

Figure 18. Tangled Fibers within a Fiber Bundle, (a) Optical Microscopy, (b) Scanning Electron Microscopy

1. Tensile Test Results

Several tensile tests were run for carbon fiber bundles with steel adapters. A representative test result is per Figure 19. The results from the tensile testing are further analyzed later while discussing slack fiber behavior.

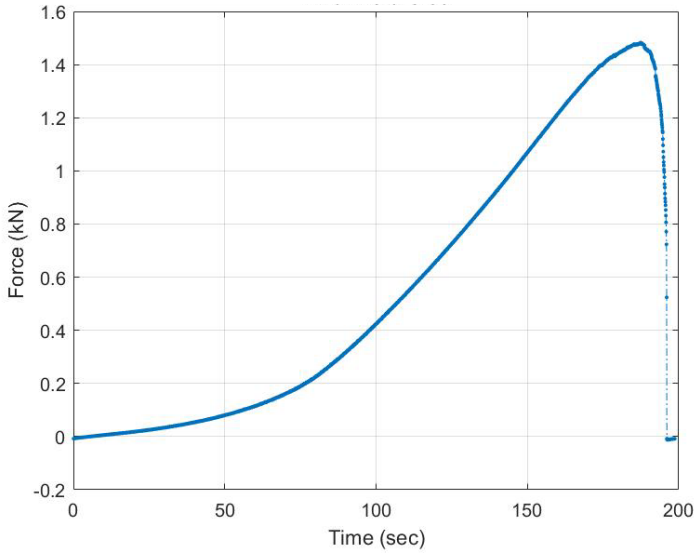

Figure 19. MTS Data for Carbon Fiber Tensile Test

2. Cyclic Test Results

The cyclic testing for carbon fiber also contributed to refinement of test methodology. Tests were conducted using both the larger polycarbonate adapters and steel adapters. Other iterations were to wrap the carbon fiber bundle around the adapter only one time instead of the more frequently used two wraps.

a. Large Polycarbonate Adapters

Tests were conducted with maximum strains from 0.03 to 0.07, in increments of 0.01. The testing at a strain rate of 0.03 had a similar result to the glass fiber testing where the minimum force increased, as in Figure 20. Therefore, it was determined that the testing at this maximum strain occurred at a displacement too low for all fibers to become taut and loaded due to the twisting in the fiber bundles. The testing with a maximum strain of 0.04 did not have an increasing lower force, but did reach a constant difference between the lower and upper force bounds, as in Figure 21. The tests with a maximum strain rate of 0.05 behaved similarly to those at 0.04, but the differential reached between the lower and upper force bounds was even smaller. The tests with a maximum strain of 0.06 were the first to reach failure, as in Figure 22. Subsequently, the tests with a maximum strain of 0.07 also reached failure. However, similar to the glass fiber results, there were still inconsistencies between tests, as in Table 4. While the maximum force reached was more consistent for each strain rate testing, there were still variations between the number of cycles it took to reach 70% and 40% of the maximum force, as shown in Figures 23 and 24.

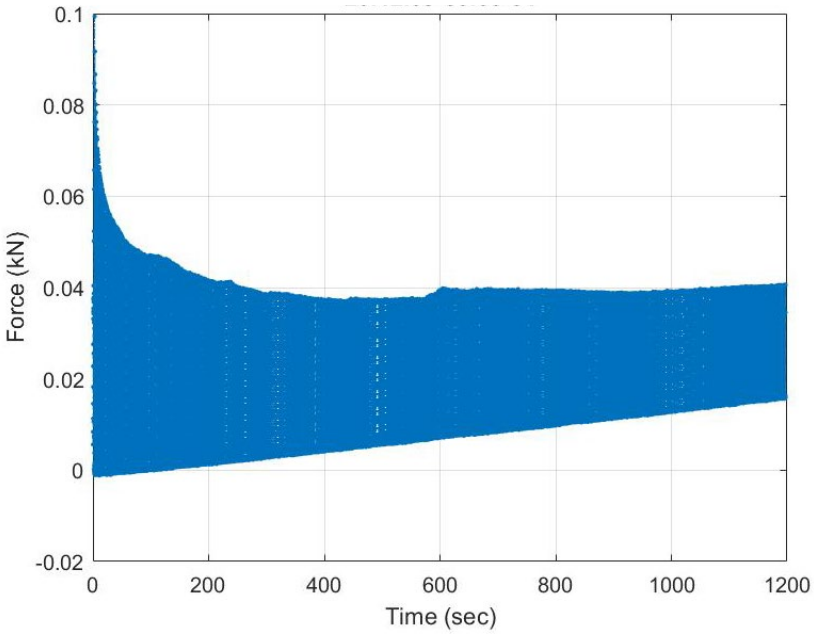

Figure 20. MTS Data for Carbon Fiber Cyclic Test with Maximum Strain of 0.03 using Large Polycarbonate Adapters

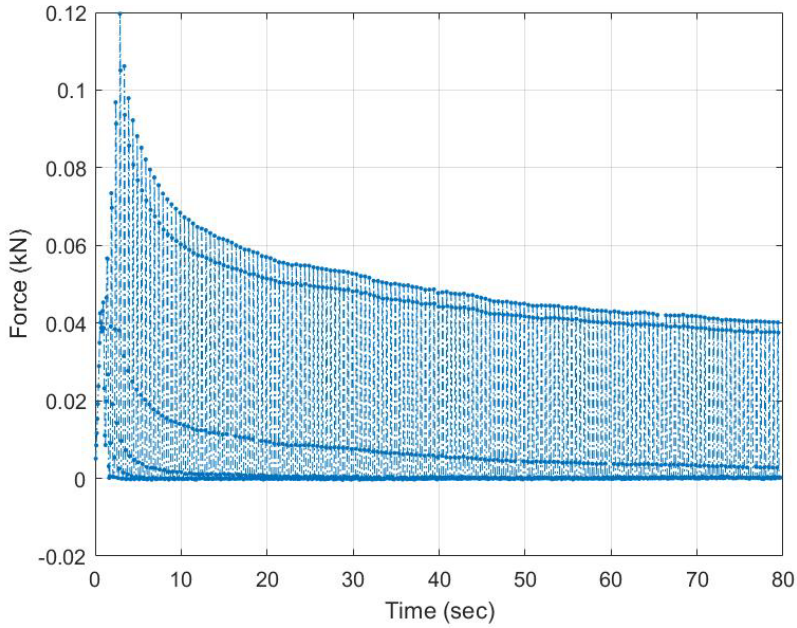

Figure 21. MTS Data for Carbon Fiber Cyclic Test with Maximum Strain of 0.04 using Large Polycarbonate Adapters

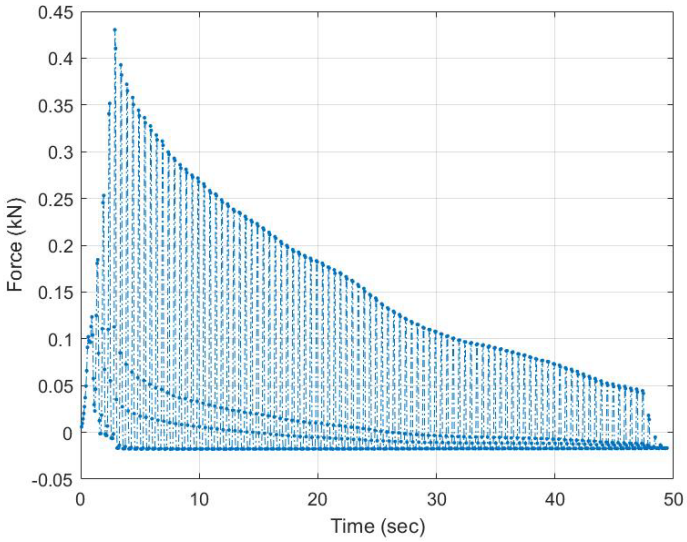

Figure 22. MTS Data for Carbon Fiber Cyclic Test with Maximum Strain of 0.06 using Large Polycarbonate Adapters

Table 4. Carbon Fiber Test Data from Strain-based Cyclic Tests Using Large Polycarbonate Adapters

Max Strain	Max Force (kN)	No. of Cycles to Peak	70% Force (kN)	No. of Cycles to 70% Force	No. of Cycles from Peak to 70% Force	40% Force (kN)	No. of Cycles to 40% Force	No. of Cycles from Peak to 40% Force
0.03	0.0994	5.89	0.0696	17.89	12.00	0.0398	521.80	515.91
0.04	0.1196	5.77	0.0837	11.77	6.00	0.0478	82.76	76.99
	0.1247	5.89	0.0873	13.89	8.00	0.0499	112.88	106.99
	0.1456	5.76	0.1019	17.76	12.00	0.0582	158.76	153.00
0.05	0.2709	5.89	0.1896	30.90	25.01	0.1084	65.90	60.01
	0.1903	5.76	0.1332	13.76	8.00	0.0761	61.76	56.00
	0.2454	5.89	0.1718	16.89	11.00	0.0982	59.88	53.99
	0.1974	5.76	0.1382	12.76	7.00	0.0790	77.76	72.00
0.06	0.2872	5.77	0.2010	11.77	6.00	0.1149	52.76	46.99
	0.4919	5.89	0.3443	23.88	17.99	0.1968	64.88	58.99
	0.4085	5.76	0.2860	15.89	10.12	0.1634	42.88	37.12
	0.2641	5.89	0.1849	17.89	12.00	0.1056	121.88	115.99
	0.4304	5.77	0.3013	14.77	9.00	0.1722	43.76	37.99
0.07	0.6549	5.89	0.4584	16.89	11.00	0.2620	26.88	20.99
	0.6773	5.76	0.4741	15.76	10.00	0.2709	25.76	20.00
	0.7749	5.89	0.5424	11.89	6.00	0.3100	14.76	8.88
	0.7208	5.76	0.5046	16.76	11.00	0.2883	24.76	19.00

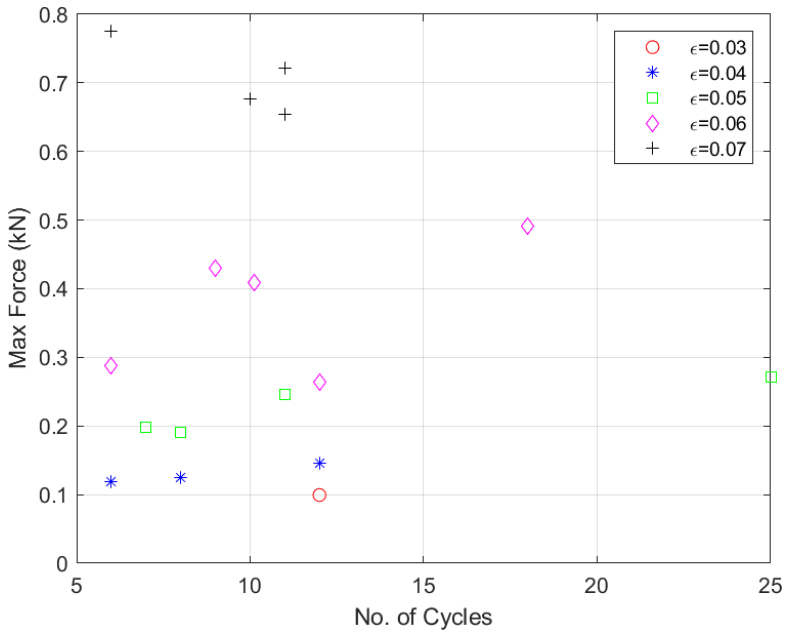

Figure 23. Carbon Fiber Evaluation at 70% of Maximum Force Across Varying Strains Using Large Polycarbonate Adapters

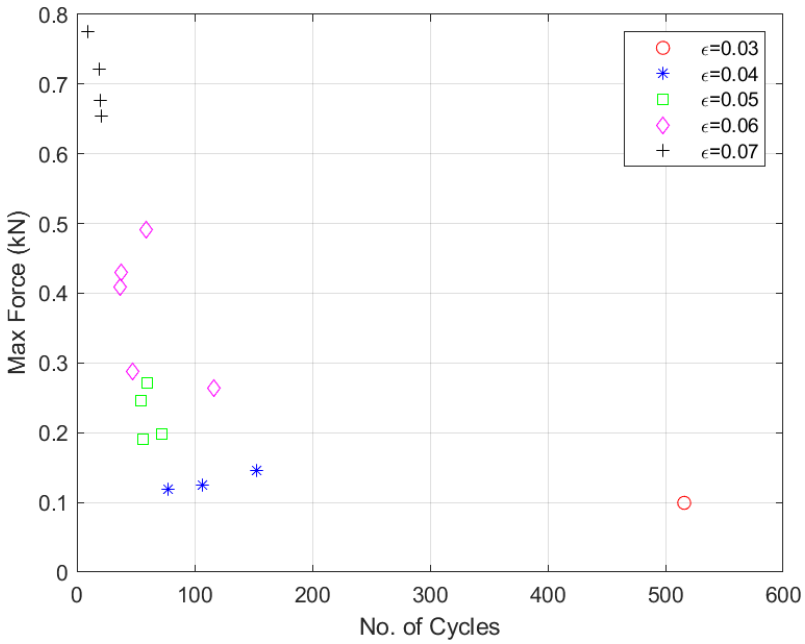

Figure 24. Carbon Fiber Evaluation at 40% of Maximum Force Across Varying Strains Using Large Polycarbonate Adapters

b. Steel Adapters

Similar to the testing conducted using the large polycarbonate adapters, testing with steel adapters was conducted with maximum strains of 0.03 to 0.07, in increments of 0.01. Additionally, at the maximum strains of 0.03 and 0.04, tests were conducted with both one and two wraps of the fiber bundle around the adapters to investigate possible differences in slippage, as per Table 5. Looking solely at the tests with two wraps, similar inconsistencies to prior testing were seen, as in Figures 25 and 26. For the evaluations at both 70% and 40% of the maximum force, there were closer correlations between data points at the lower maximum strains of 0.03 and 0.04 than at the higher maximum strains between 0.05 and 0.07. Additionally, tests were run with the fiber bundle wrapped both once and twice around the adapter for the maximum strains of 0.03 and 0.04. Maximum force reached and number of cycles to reach both 70% and 40% of the maximum force were evaluated, as in Figures 27 and 28. The tests with two wraps of the fiber bundles led to much closer correlations in the number of cycles. Therefore, the determination was made that two wraps is a better test methodology as it likely leads to less slippage. While using the steel adapters solved the issue of adapter deflection, the inconsistencies in test data still warranted further examination into test methodology. With a strain-based cyclic test, the entire test is conducted undergoing the same displacement. However, as the fibers become either elastically deformed during the test run or plastically deformed once individual fibers begin to fail, the displacement is still the same. This is why some of the strain-based cyclic tests run at lower maximum strains never reach failure, as the displacement never results in the test exceeding the failure strength of the material.

Table 5. Carbon Fiber Test Data from Strain-based Cyclic Tests Using Steel Adapters

Max Strain / No. of Wraps	Max Force (kN)	No. of Cycles to Peak	70% Force (kN)	No. of Cycles to 70% Force	No. of Cycles from Peak to 70% Force	40% Force (kN)	No. of Cycles to 40% Force	No. of Cycles from Peak to 40% Force
0.03/ 2 wraps	0.1599	5.76	0.1119	9.76	4.00	0.0640	31.76	26.00
	0.0661	5.77	0.0463	8.77	3.00	0.0264	31.76	25.99
	0.1412	5.76	0.0988	9.76	4.00	0.0565	35.76	30.00
	0.0776	5.89	0.0543	9.89	4.00	0.0310	44.90	39.01
0.03/ 1 wrap	0.0665	5.76	0.0466	10.76	5.00	0.0266	110.76	105.00
	0.1375	5.89	0.0963	15.89	10.00	0.0550	663.80	657.91
	0.1286	5.89	0.0900	9.89	4.00	0.0514	38.90	33.01
	0.1636	5.77	0.1145	9.77	4.00	0.0654	75.76	69.99
0.04/ 2 wraps	0.1213	5.89	0.0849	9.89	4.00	0.0485	35.90	30.01
	0.0913	5.89	0.0639	8.89	3.00	0.0365	31.88	25.99
	0.2981	5.77	0.2087	10.77	5.00	0.1192	37.76	31.99
	0.1500	5.77	0.1050	8.77	3.00	0.0600	23.76	17.99
0.04/ 1 wrap	0.9546	5.77	0.6682	23.76	17.99	0.3818	37.76	31.99
	0.8310	5.77	0.5817	32.76	26.99	0.3324	68.76	62.99
	0.6808	5.89	0.4766	28.88	22.99	0.2723	48.88	42.99
0.05/ 2 wraps	0.4048	5.89	0.2834	10.89	5.00	0.1619	37.90	32.01
	0.2768	5.76	0.1938	10.89	5.12	0.1107	77.88	72.12
	0.2410	5.89	0.1687	11.89	6.00	0.0964	80.90	75.01
	0.2624	5.77	0.1837	9.77	4.00	0.1050	36.76	30.99
	0.4451	5.89	0.3116	17.89	12.00	0.1780	121.90	116.01
	0.2363	5.76	0.1654	9.76	4.00	0.0945	50.76	45.00
	0.5202	5.89	0.3641	11.89	6.00	0.2081	34.90	29.01
0.06/ 2 wraps	0.2766	5.89	0.1936	12.89	7.00	0.1106	97.90	92.01
	0.5839	5.89	0.4087	17.89	12.00	0.2336	44.88	38.99
	0.4515	5.89	0.3161	11.89	6.00	0.1806	52.88	46.99
	0.7587	5.89	0.5311	21.88	15.99	0.3035	49.88	43.99
0.07/ 2 wraps	1.2400	5.89	0.8680	11.89	6.00	0.4960	15.76	9.88
	1.2970	5.76	0.9079	16.76	11.00	0.5188	32.76	27.00
	0.8210	5.76	0.5747	13.76	8.00	0.3284	30.76	25.00

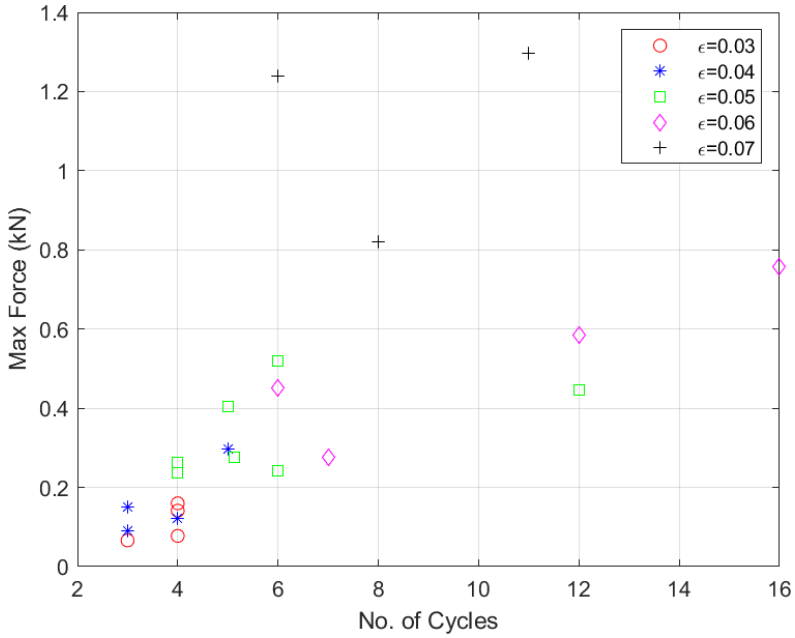

Figure 25. Carbon Fiber Evaluation at 70% of Maximum Force Across Varying Strains Using Steel Adapters

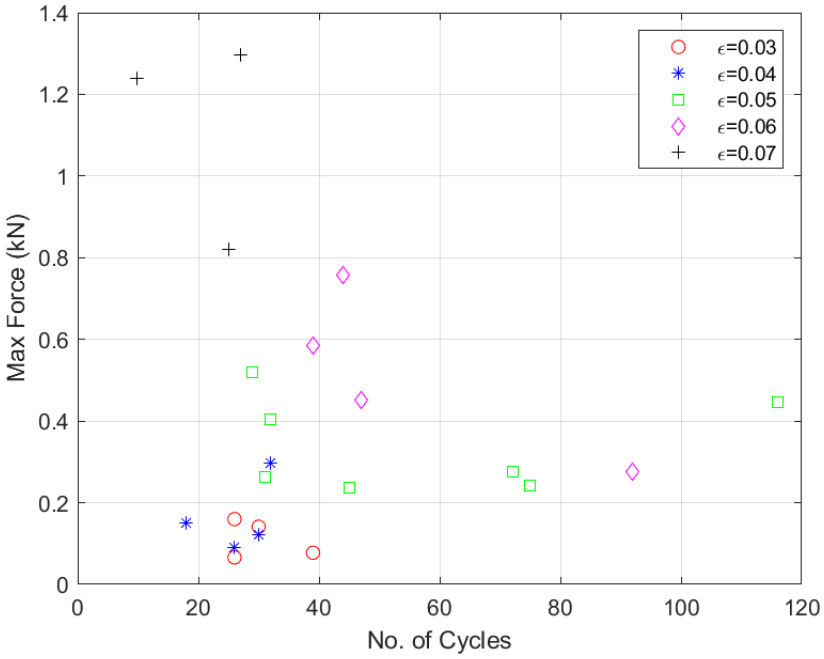

Figure 26. Carbon Fiber Evaluation at 40% of Maximum Force Across Varying Strains Using Steel Adapters

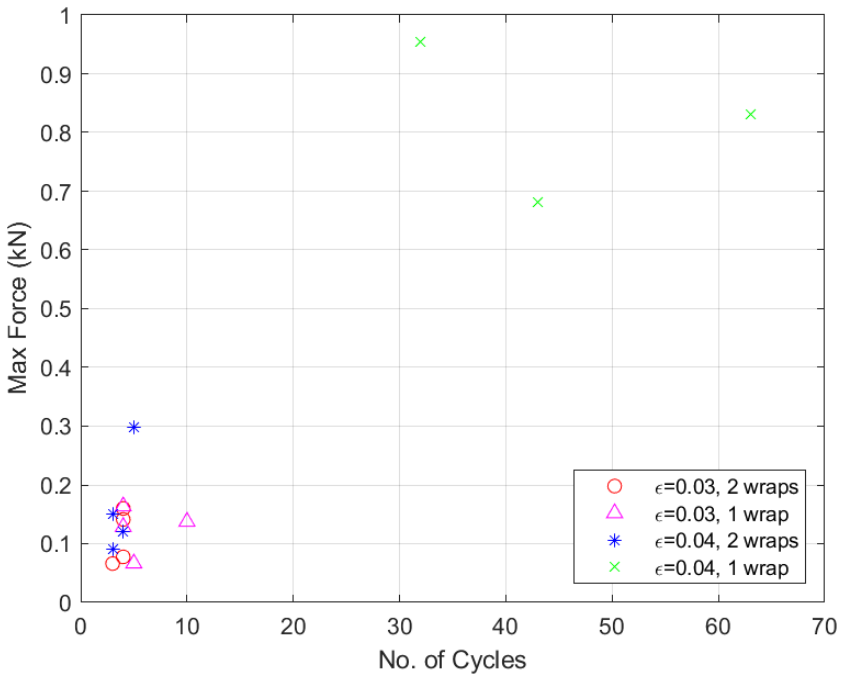

Figure 27. Carbon Fiber Evaluation of No. of Wraps at 70% of Maximum Force for Strains of 0.03 and 0.04 Using Steel Adapters

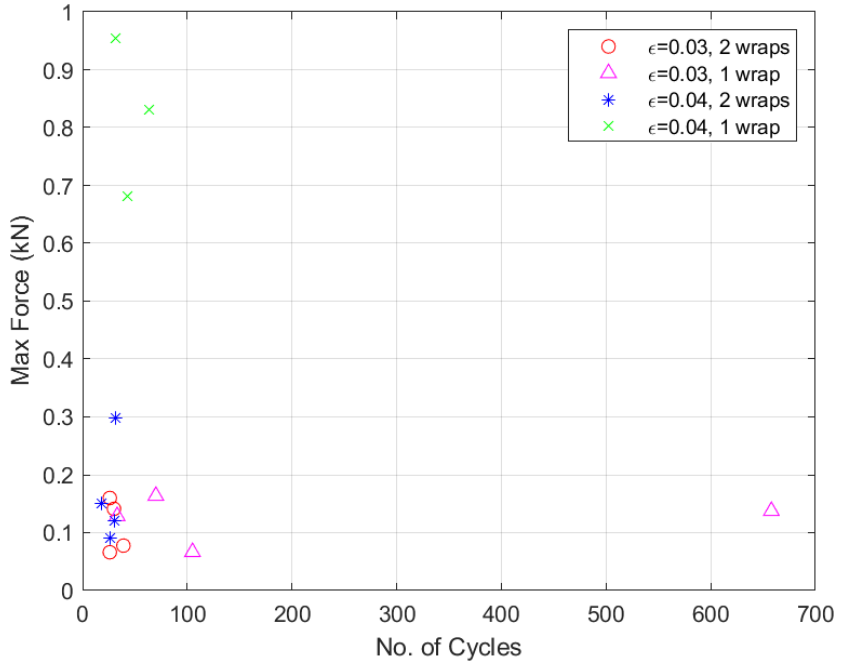

Figure 28. Carbon Fiber Evaluation of No. of Wraps at 40% of Maximum Force for Strains of 0.03 and 0.04 Using Steel Adapters

3. Multi-part Test Results

The three material characteristics taken for analysis from the multi-part tests were residual failure strength, Young's modulus, and failure strain. These characteristics were found utilizing stress-strain curves created from the data from the tensile portion of the testing, as per Figure 29. All of the multi-part tests were conducted using steel adapters in the horizontal orientation. In order to determine characteristics under tensile loading only, three tensile tests were conducted with this adapter/orientation configuration prior to the multi-part testing and the results were then averaged, as per Table 6. The average values were used as the 0 cycle data point for analysis in both the strain and force-based tests.

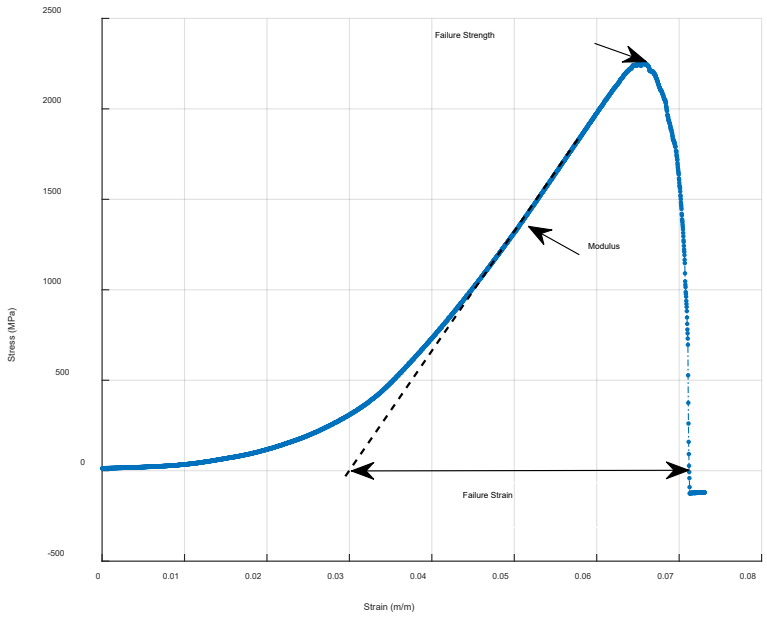

Figure 29. Plot Demonstrating Material Characteristics from Tensile Testing. Source: [21].

Table 6. Carbon Fiber Tensile Data with Steel Adapters

	Failure Strength (MPa)	E (GPa)	Failure Strain (mm/mm)
Test 1	2734	64.35	0.0451
Test 2	2552	61.99	0.0432
Test 3	2606	61.74	0.0444
Average	2631	62.69	0.0443

a. Strain-based

For the strain-based multi-part testing, the cyclic portions were all conducted with a maximum strain of 0.05. The cyclic portions were run for between 2000 to 11000 cycles, in increments of 1000 cycles. The same characteristics as in Table 6 were calculated, and in addition, were non-dimensionalized using the average values as in Table 6. The results are per Table 7.

Table 7. Material Properties from Multi-part Strain-based Testing with a Maximum Strain of 0.05

	Failure Strength		E		Failure Strain	
No. of Cycles	(MPa)	(nondim)	(GPa)	(nondim)	(mm/mm)	(nondim)
0	2630.7	1.000	62.69	1.000	0.0443	1.000
2000	730.0	0.277	33.61	0.536	0.0321	0.725
3000	253.5	0.096	16.89	0.269	0.0181	0.410
4000	323.8	0.123	13.73	0.219	0.0300	0.679
5000	568.8	0.216	22.89	0.365	0.0280	0.634
6000	353.0	0.134	17.03	0.272	0.0259	0.584
7000	569.2	0.216	27.90	0.445	0.0207	0.467
8000	826.2	0.314	32.38	0.517	0.0292	0.660
8000	608.9	0.231	34.70	0.554	0.0224	0.505
9000	717.0	0.273	27.66	0.441	0.0289	0.654
9000	62.2	0.024	6.65	0.106	0.0108	0.244
10000	88.3	0.034	6.67	0.106	0.0177	0.400
10000	409.0	0.155	15.54	0.248	0.0297	0.671
11000	366.0	0.139	22.38	0.357	0.0170	0.384

b. Force-based

For the force-based multi-part testing, a maximum force of 1kN was the system input. However, of note, these tests all peaked at approximated 960 N during the cyclic portion. Additionally, as noted earlier, these tests were conducted at a slower test rate of 0.25 Hz in order to as close as feasible match the inputted force. The cyclic portions were run for between 250 to 1500 cycles, in increments of 250 cycles. The results are per

Table 8. Additionally, for running a force-based cyclic test all the way to failure, the number of cycles to failure was determined to be 1510.8 cycles.

Table 8. Material Properties from Multi-part Force-based Testing with a Maximum Force of 1 kN

	Failure Strength		E		Failure Strain	
No. of Cycles	(MPa)	(nondim)	(GPa)	(nondim)	(mm/mm)	(nondim)
0	2630.7	1.000	62.69	1.000	0.0443	1.000
250	2934.0	1.115	111.88	1.785	0.0313	0.708
250	2618.0	0.995	123.59	1.971	0.0275	0.621
500	2844.0	1.081	116.71	1.862	0.0291	0.658
500	2559.0	0.973	114.96	1.834	0.0258	0.583
750	2750.0	1.045	123.64	1.972	0.0267	0.603
750	2460.0	0.935	113.93	1.817	0.0248	0.561
1000	2902.0	1.103	117.81	1.879	0.0301	0.681
1000	2638.0	1.003	116.25	1.854	0.0261	0.590
1250	1981.0	0.753	119.96	1.913	0.0189	0.428
1250	2404.0	0.914	117.63	1.876	0.0237	0.535
1500	2386.0	0.907	121.44	1.937	0.0225	0.508

THIS PAGE INTENTIONALLY LEFT BLANK

IV. MATHEMATICAL MODEL FORMULATION AND ANALYSIS

A. SLACK FIBER BEHAVIOR IN TENSILE TESTS

As mentioned earlier, fiber bundles were not necessarily evenly loaded due to the fact that the twisted nature of the bundles left more slack in some fibers at the start of testing. This is evidenced by the small but gradually increasing initial slope, as in Figure 30. The second portion of the diagram with the constant slope, and therefore constant elastic modulus, occurs when all fibers in the bundle are carrying load. The third portion leading to failure has a decreasing slope, as a result of individual fibers beginning to fail prior to complete failure of the bundle. These fibers that fail sooner are likely the fibers that had the smallest amount of slack during initial loading and therefore were more heavily loaded sooner in the test. Because the fibers are not all equally loaded from the start of the test, the maximum strength seen is lower than the strength should an equally loaded fiber bundle undergo testing, as in Table 9. For the experimental data, the test data in terms of force and time, as in Figures 14 and 19, was converted to a stress-strain curve using, respectively,

$$\sigma = \frac{F}{A}$$

and

$$\varepsilon = \frac{(Time)(Testing\_Rate)}{L}$$

In order to make a prediction of slack fiber behavior, a probability function, *p(s)*, was used to represent the fraction of fibers in a bundle that had an initial slack length of *s*. As a probability function, it must satisfy the expression [21]:

$$\int_0^\infty p(s)ds = 1$$

As the load is applied, the force exerted on fibers with a slack length less than the displacement is expressed as [21]:

$$F(\delta) = \int_0^{s_m} k \langle \delta - s \rangle p(s) ds$$

with

$$\langle \delta - s \rangle = \begin{cases} \delta - s & if \ \ \delta \geq s \\ 0 & if \ \ \delta < s \end{cases}$$

The equivalent spring constant of the fiber, k, is calculated by

$$k = \frac{AE}{L}$$

where A is the cross-section area, E is the elastic modulus, and L is the length [21]. The values for these parameters are per Table 9. A skewed normal distribution was assumed in order to define the probability function:

$$p(s) = \phi\left(\frac{s-\xi}{\omega}\right)\Phi\left(\alpha\frac{s-\xi}{\omega}\right)$$

with

$$\phi\left(\frac{s-\xi}{\omega}\right) = \frac{1}{\pi\omega} e^{-\frac{(s-\xi)^2}{2\omega^2}}$$

and

$$\Phi\left(\alpha\frac{s-\xi}{\omega}\right) = \int_{-\infty}^{\alpha\left(\frac{s-\xi}{\omega}\right)} e^{-\frac{t^2}{2}} dt$$

where α is the skewness of the probability function and ξ and ω are the mean and standard deviation, respectively, is there was no skewness (α=0) [21]. The values for these parameters are per Table 9. This modeling was done for both carbon and glass fibers, as

per Figures 30 and 31, respectively. In both cases, the experimental data provided a close correlation to the model. Of note, the skewness for both cases was the same.

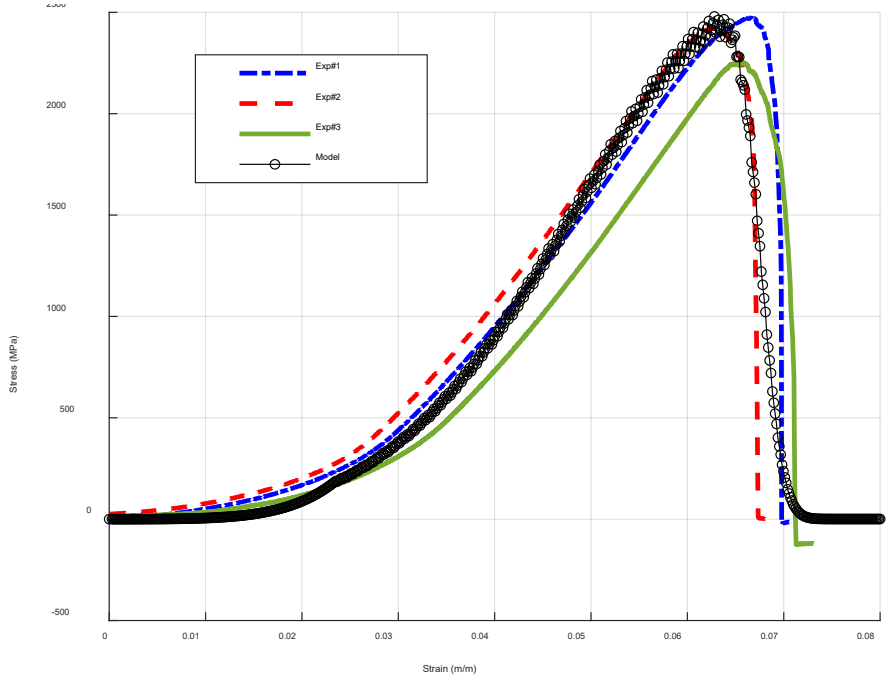

Figure 30. Comparison of Tensile Tests of between Experimental and Model for Carbon Fiber Bundles. Source: [21].

Table 9. Parameters for Slack Model. Adapted from [21].

		Carbon fibers	Glass fibers
Material Properties	Elastic Modulus – E (GPa)	230	72
	Failure Strength (GPa)	5.3	1.45
Geometric Properties	Length – L (mm)	93	65
	Area – A (mm^2)	0.60	0.45
Parameters for Skewed Normal Distribution	Skewness – α	-11	-11
	Positive scale – ω (mm)	$1.8x10^{-3}$	$2.7x10^{-3}$
	Location – ξ (mm)	6.3	7.7

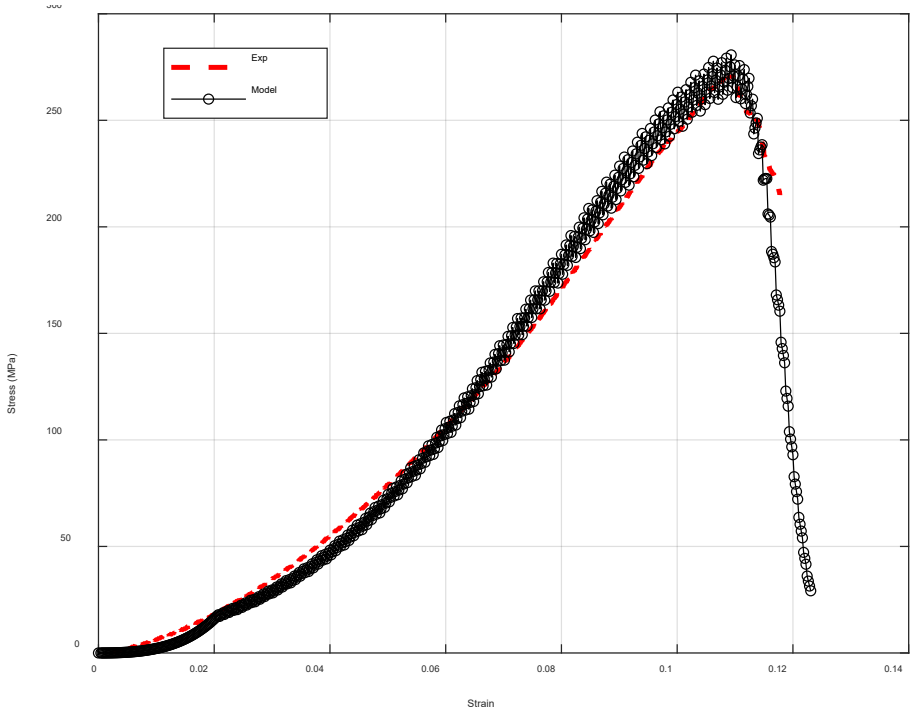

Figure 31. Comparison of Tensile Tests of between Experimental and Model for Glass Fiber Bundles. Source: [21].

B. MATHEMATICAL MODELING FOR MULTI-PART TESTS

1. Strain-based

For the material characteristics of residual failure strength, Young's Modulus, and failure strain, a decreasing exponential function provided the best fit:

$$\frac{f(n)}{f_o} = e^{-cn^d}$$

where n is the number of cycles, f_o is the function value at zero cycles in order to non-dimensionalize, and c and d are constants used to fit the curve. In each case, setting d to 0.25 provided the best fit. However, c varied for each characteristics, as demonstrated in Figures 32–34. Of note though, documenting the number of cycles to failure requires further analysis due to the inconsistencies that were previously discussed.

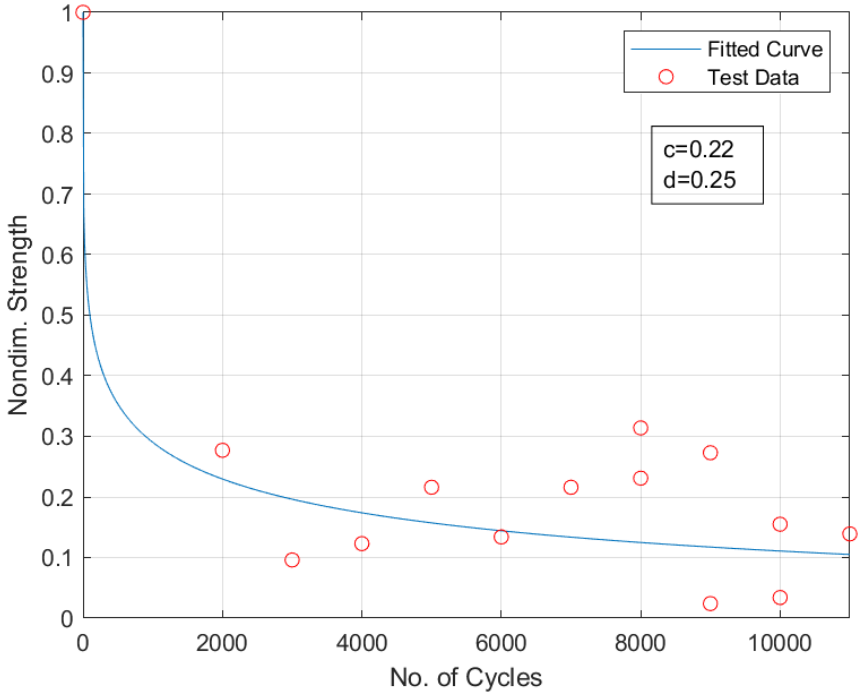

Figure 32. Residual Failure Strength Model for Strain-based Testing

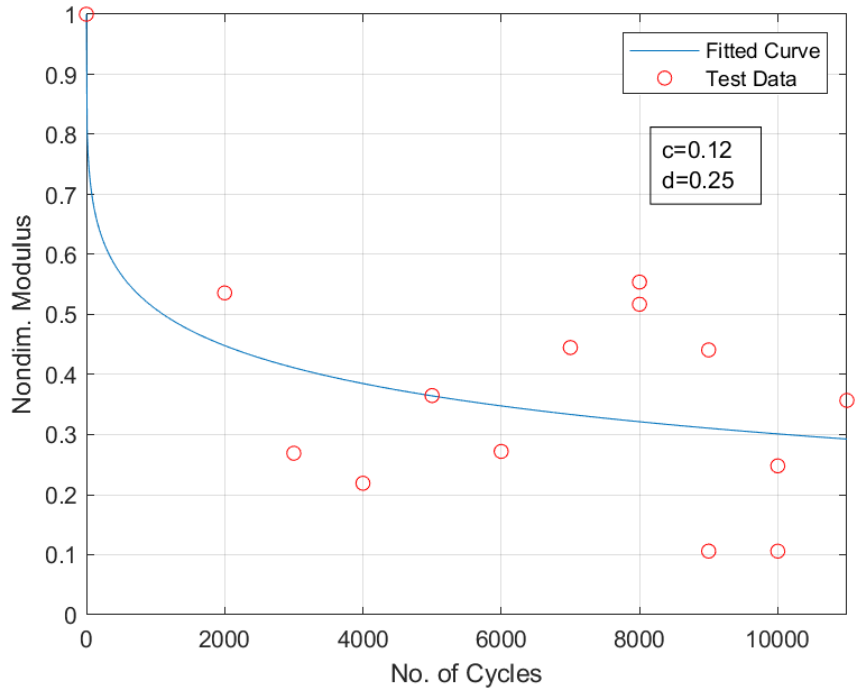

Figure 33. Young's Modulus Model for Strain-based Testing

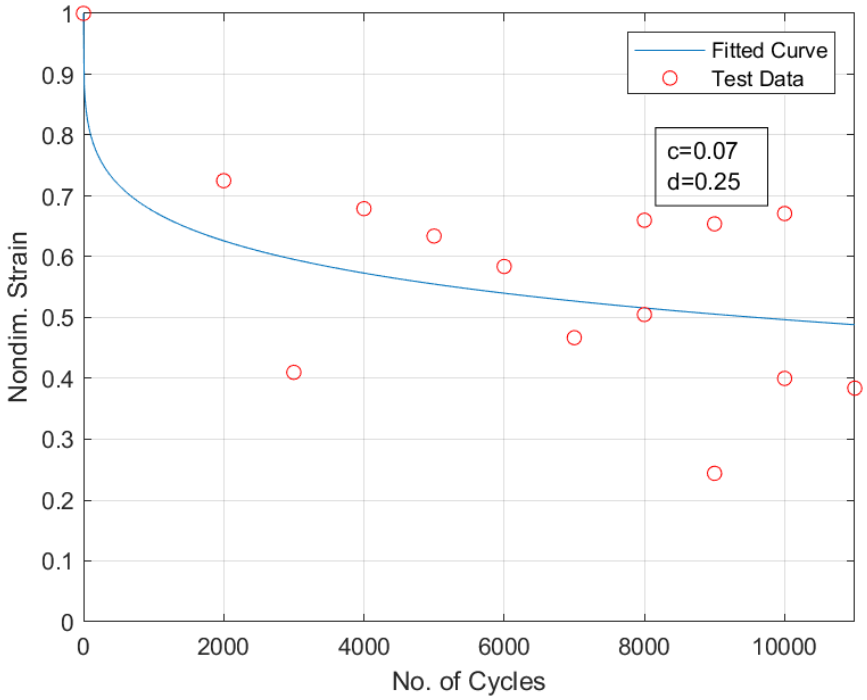

Figure 34. Failure Strain Model for Strain-based Testing

2. Force-based

For the material characteristic of residual failure strength, the data was better fitted by the following function:

$$\frac{f(n)}{f_o} = 1 - e^{\frac{n-n_f}{c}}$$

where n is the number of cycles, n_f is the number of cycles to failure (1510.8 cycles for this set of test data), f_o is the function value at zero cycles in order to non-dimensionalize, and c is the constant used to fit the curve. This result is as per Figure 35. For the material characteristic of Young's Modulus, all of the experimental values were above the tensile test value and also had inconsistencies, so additional work on this would need to be conducted prior to mathematical modeling being feasible. For the material characteristic of residual failure strain, the same modeling as used for the strain-based analysis provided the best fit. However, both constants had different values than in the residual failure strength in the strain-based testing, as per Figure 36.

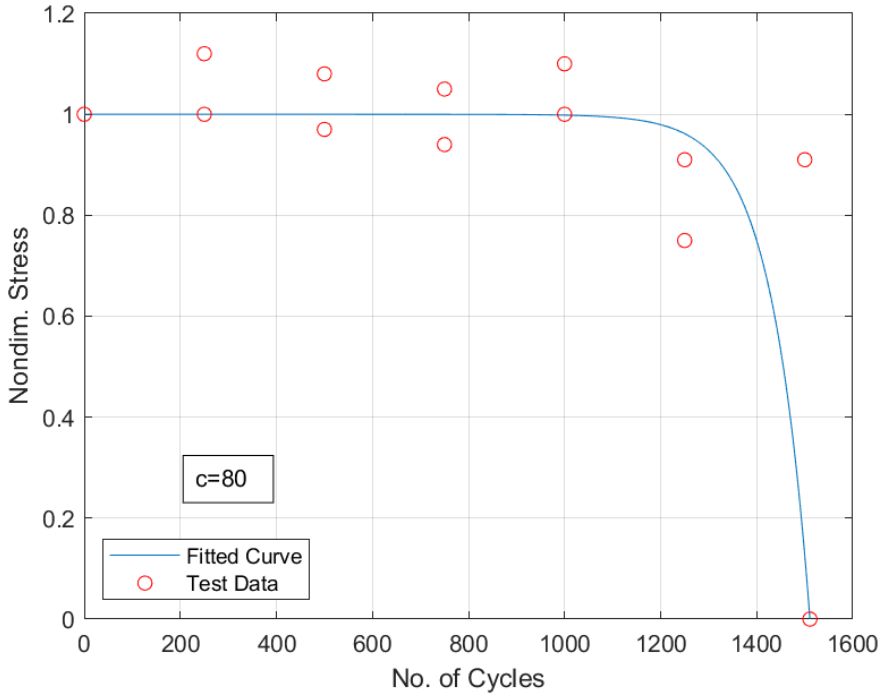

Figure 35. Residual Failure Strength Model for Force-based Testing

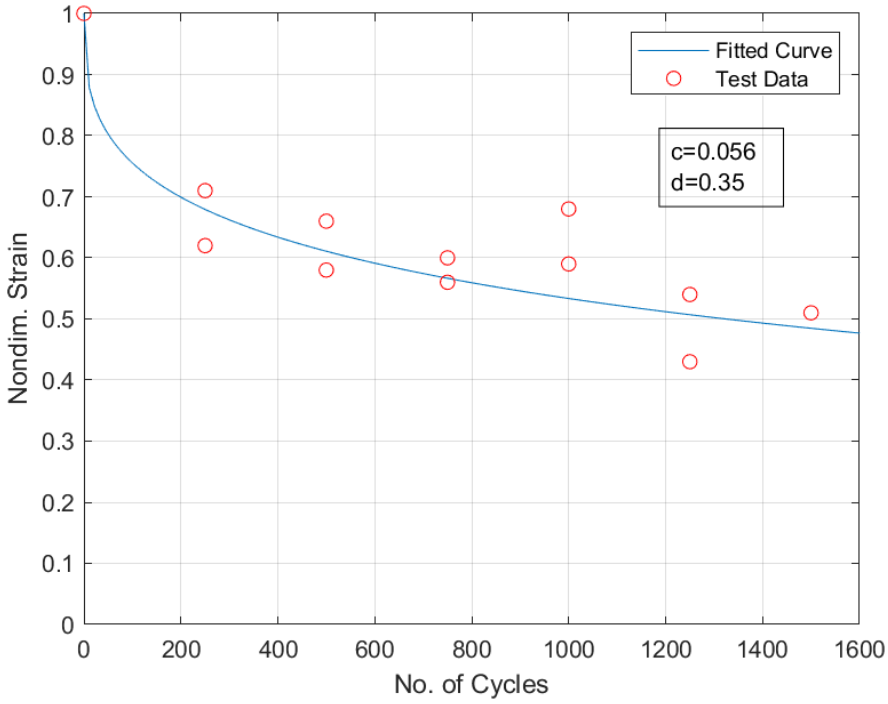

Figure 36. Failure Strain Model for Force-based Testing

THIS PAGE INTENTIONALLY LEFT BLANK

V. CONCLUSIONS AND FUTURE WORK

A. CONCLUSIONS

The ultimate goal to which this research contributes is to utilize a multiscale model to predict fatigue failure of composites using micro-scale testing, a methodology described in [19]. The focus of this study was to conduct micro-scale testing on the fiber bundles, which could be manufactured into a composite along with a binder/matrix. A significant portion of the research also contributed to the refinement of test methodology. Glass fiber and carbon fiber bundles were both subjected to tensile testing and strain-based cyclic testing. Carbon fiber bundles were also subjected to multi-part testing, which involved conducting a strain-based or force-based cyclic test for a predetermined number of cycles and then conducting a subsequent tensile test until sample failure. Additionally, four different adapters for mounting the fiber bundles into the test machine were utilized in order to find one that underwent a sufficiently small amount of deflection.

The first two adapter types, PLA and polycarbonate with the smaller geometry, both visibly deflected during testing. Additionally, the PLA adapters compressed under the grip strength of the MTS. While the polycarbonate adapters with the larger geometry did not visibly deflect, they still did not meet the desired maximum deflection of 0.1 mm when an FEA was conducted. The steel adapters were the only type that met the desired maximum deflection of 0.1 mm.

The fiber bundles were observed to be arranged in a tangled manner rather than in a linear manner. This resulted in some fibers still having slack at the commencement of a test. In order to make a prediction of the slack fiber behavior, a probability function was used to represent the fraction of fibers in a bundle that had a certain initial slack length. A skewed normal distribution was assumed to define the probability function. This modeling provided a close correlation to the tensile test data for both the glass fiber and carbon fiber bundles.

Cyclic testing required more refinement of the test methodology. For the glass fiber bundles, strain-based cyclic testing was conducted using the large polycarbonate adapters.

For the carbon fiber bundles, strain-based cyclic testing was conducted using both the large polycarbonate adapters and the steel adapters. In all cases, tests were run for maximum strains from 0.03-0.07. However, there were inconsistencies in the results of the data. The biggest inconsistencies were in the number of cycles it took to reach 70% and 40% of the maximum force for each maximum strain. Additionally, there was variation in the maximum force reached, especially in the tests using the large polycarbonate adapters. This is likely a result of the test methodology. In the strain-based testing, the distance between the minimum and maximum points of the cycle is held constant. However, as the fibers undergo deformation, whether it be elastic during a test run or plastic once individual fibers begin to fail, the force applied will be decreasing.

The final test methodology was to conduct multi-part tests, with a cyclic test followed by a tensile test to failure. This allowed for evaluation of the residual strength in a sample following cyclic testing for a specified number of cycles. Of note, these tests were all conducted using carbon fiber bundles and steel adapters. Two sets of multi-part tests were conducted, one strain-based with a maximum strain of 0.05 and one force-based with a maximum force of 1 kN. Three material characteristics were examined: residual failure strength, Young's Modulus, and failure strain. For the strain-based testing, these were all well correlated using the mathematical modeling. However, for the force-based testing, while residual failure strength and failure strain were well correlated using the mathematical modeling, Young's Modulus was not. From the experimental data, the Young's modulus data for any of the multi-part testing was greater than the Young's Modulus found during pure tensile testing. Therefore, this material characteristic would require further investigation.

B. FUTURE WORK

This study was limited to the collection of data for only certain force and strain parameters. The next effort would be to vary the strain or force for the cyclic portion of the testing in order to compare plots. The goal of this would be to develop a scalable relationship for varying the cyclic test parameter. Essentially, taking the same base equations, the goal would be to know the relationship by which to scale the constants based

on the change in the strain or force parameter. Also, further examination into Young's Modulus during force-based testing is needed. Additionally, further study into the multi-scale approach is needed. Since this testing was on the fiber bundles only, testing on the matrix alone also needs to be conducted. These results can then be combined with the fiber results using the multi-scale approach in order to predict the behavior of the overall composite in fatigue failure.

THIS PAGE INTENTIONALLY LEFT BLANK

LIST OF REFERENCES

[1] Strong, A., 2008, "Introduction to Composites," *Fundamentals of Composites Manufacturing: Materials, Methods, and Applications, Society of Manufacturing Engineers*, pp. 1–18.

[2] Jareteg, C. et al., 2016, "Geometry Assurance Integrating Process Variation with Simulation of Spring-In for Composite Parts and Assemblies," *Journal of Computing and Information Science in Engineering*, 16(3), pp. 031003-1 - 031003-7.

[3] Rubino, F., Nisticò, A., Tucci, F., and Carlone, P., 2020, "Marine Application of Fiber Reinforced Composites: A Review," *Journal of Marine Science and Engineering*, 8(26).

[4] Bielawski, R., 2017, "Composite Materials in Military Aviation and Selected Problems with Implementation," *Review of the Air Force Academy*, 1(33).

[5] Sloan, J., ed., "Skinning the F-35 Fighter," Composites World, last modified October 19, 2009, https://www.compositesworld.com/articles/skinning-the-f-35-fighter.

[6] "Composite Aircraft Structure," Federal Aviation Administration, AC 20–107B, September 2009.

[7] Findlay, S. J. and Harrison, N. D., 2002, "Why Aircraft Fail," *Materials Today*, 5(11), pp. 18–25.

[8] Callister, Jr., W. D. and Rethwisch, D. G., 2010, *Materials Science and Engineering, An Introduction*, John Wiley & Sons, Inc., Hoboken, NJ.

[9] Hahn, H. T. and Kim, R. Y., Jul. 1975, "Proof Testing of Composite Materials," *Journal of Composite Materials*, 9, pp. 297–311.

[10] Hwang, W. and Han, K. S., Mar. 1986, "Fatigue of Composites—Fatigue Modulus Concept and Life Prediction," *Journal of Composite Materials*, 20(2), pp. 154–165.

[11] Tay, T. E., Liu, G., Yudhanto, A., and Tan, V. B. C., 2008, "A Micro—Macro Approach to Modeling Progressive Damage in Composite Structures," *International Journal of Damage Mechanics*, 17(1), pp. 5–28.

[12] Kassapoglou, C., 2007, "Fatigue Life Prediction of Composite Structures Under Constant Amplitude Loading," *Journal of Composite Materials*, 41(22), pp. 2737–2754.

[13] Diao, X., Ye, L., and Mai, Y. W., Jan. 1995, "A Statistical Model of Residual Strength and Fatigue Life of Composite Laminates," *Composites Science and Technology*, 54(3), pp. 329–336.

[14] Zakaria, K. A. et al., Dec. 2016, "Study on Fatigue Life and Fracture Behaviour of Fibreglass Reinforced Composites," *Journal of Mechanical Engineering and Sciences*, 10(3), pp. 2300–2310.

[15] Chou, P. C. and Croman, R., Jul. 1978, "Residual Strength in Fatigue Based on the Strength-Life Equal Rank Assumption," *Journal of Composite Materials*, 12 (2), pp. 177–194.

[16] Yang, J. N. and Liu, M. D., Apr. 1977, "Residual Strength Degradation Model and Theory of Periodic Proof Tests for Graphite/Epoxy Laminates," *Journal of Composite Materials*, 11(2), pp. 176–203.

[17] Wang, S. S. and Chim, E. S. M., Mar. 1983, "Fatigue Damage and Degradation in Random Short-Fiber SMC Composite," *Journal of Composite Materials*, 17, pp. 114–134.

[18] Talreja, R., 2008, "Damage and Fatigue in Composites – A Personal Account," *Composites Science and Technology*, 68, pp. 2585–2591.

[19] Kwon, Y. W. and Darcy, J., 2017, "Failure Criteria for Fibrous Composites Based on Multiscale Modeling," *Multiscale and Multidisciplinary Modeling, Experiments and Design*, 1, pp. 3–17.

[20] Haller, C., 2020, "Study of Fatigue Failure of Composite Materials," Thesis, Naval Postgraduate School, Monterey, CA.

[21] Kadlec, L., Kwon, Y. W., Haller, C., Park, C.-M., and Didoszak, J. M., 2021, "Tensile and Cyclic Loading of Fiber Bundles," *Multiscale and Multidisciplinary Modeling, Experiments and Design*, 4, pp. 245–257.

INITIAL DISTRIBUTION LIST

1. Defense Technical Information Center
   Ft. Belvoir, Virginia

2. Dudley Knox Library
   Naval Postgraduate School
   Monterey, California